# STUDY OF THE PERFORMANCE DATA OF TRIPLE AXIS SPECTROMETER AND DETERMINATION OF MAGNETIC STRUCTURE OF Ni-Zn FERRITE

A Thesis Submitted To The Department Of Physics,
Bangladesh University Of Engineering And Technology
In Partial Fulfillment Of The Requirements For The Degree Of M.Phil.

BY

SK. MD. YUNUS

OCTOBER 1994

ROLL NO. P-9007
SESSION 1988-89

535.94

BANGLADESH UNIVERSITY OF ENGINEERING AND TECHNOLOGY
DEPARTMENT OF PHYSICS
CERTIFICATION OF THESIS WORK

A THESIS ON

STUDY OF THE PERFORMANCE DATA OF TRIPLE AXIS SPECTROMETER AND DETERMINATION OF MAGNETIC STRUCTURE OF Ni-Zn FERRITE.

BY
SK. MD. YUNUS

has been accepted as satisfactory in partial fulfilment for the degree of Master of Philosophy in physics and certify that the student demonstrated a satisfactory knowledge of the field covered by this thesis in an oral examination held on 16-10-94.



BOARD OF EXAMINERS

1. Dr.M.Ali Asgar
   Professor
   Department of Physics
   BUET.,Dhaka, Bangladesh
   — Supervisor and Chairman

2. Dr.Farid uddin Ahmed
   Principal Scientific Officer
   INST, Atomic Energy Research
   Establishment, Savar, Dhaka.
   — Co-supervisor and Member

3. Dr.Gias Uddin Ahmad
   Professor
   Department of Physics
   BUET, Dhaka, Bangladesh
   — Member

4. Dr.Tafazzal Hossain
   Professor and Head
   Department of Physics
   BUET, Dhaka, Bangladesh
   — Member

5. Dr.Abu Abdullah Ziauddin Ahmad
   Chairman,
   SPARRSO,
   Sher-e-Bangla Nagar, Dhaka.
   — Member(External)

## DECLARATION

This thesis has been done by the candidate himself and does not contain any material extracted from elsewhere or from a work published by any body else. The work of this thesis has not been presented by the candidate for another degree or diploma in any other University. No other person's work has been used without due acknowledgement.

( Sk. Md. Yunus )

**Candidate**

## CERTIFICATE

This is to certify that the research work embodying this thesis has been carried out under our supervision in the Neutron Scattering Laboratory, Institute of Nuclear Science and Technology, Bangladesh Atomic Energy Commission, Dhaka. The research work presented herein is original. This thesis has not been submitted for the award of any other degree or diploma in any other University.

M. A. Asgar

( Dr. M. Ali Asgar )

Supervisor

Professor, Department of Physics,
Bangladesh University of Engineering
and Technology

( Dr. Farid Uddin Ahmed )

Co-Supervisor

Principal Scientific Officer
Institute of Nuclear Science and Technology
Bangladesh Atomic Energy Commission

# ACKNOWLEDGEMENT

*The author has the pleasure to express his sincerest gratefulness and heartfelt thanks to his Supervisor* ***Dr. M. Ali Asgar****, Professor, Department of Physics and Dean, Faculty of Engineering, Bangladesh University of Engineering and Technology ( BUET ) for his indispensable guidance and supervision throughout this research work. The author wishes to express his utmost gratitude to the Co-Supervisor,* ***Dr. Farid Uddin Ahmed****, Principal Scientific Officer and Group Leader of Neutron Scattering Group, Institute of Nuclear Science and Technology ( INST ), Atomic Energy Research Establishment ( AERE ), for his supervision and at the same time extending his cooperation and continuous help as Group Leader of Neutron Scattering Group without which this work would not have been possible.*

*The author expresses his sincere gratitude to Dr. Tafazzal Hossain, Professor and Head, and Dr. Gias Uddin Ahmad, Professor, Department of Physics, BUET, for their constant encouragement and keen interest in the work. The author wishes to thank to all other teachers of the Physics Department, BUET, for their valuable teachings and advice during the course work and encouragement for the research. Thanks are also due to all the employees of the Department of Physics and Faculty of Engineering, BUET. The author expresses his sincere thanks to the members of the Department of Metallurgy, BUET, especially to Dr. Ehsanul Huq, Professor of the same Department for their cooperation and help.*

*The work has been done mostly in the Neutron Scattering laboratory of Reactor and Neutron Physics Division ( RNPD ) at INST, AERE, Savar, Dhaka, where the author is presently working. The author wishes to express his gratefulness to Dr. Nurul Islam Molla,*

*Director, INST, and Dr. Mizanur Rahman, Head, RNPD for their encouragement and helps. The author wishes to take opportunity in expressing his thanks to all of the members of the Neutron Scattering Group for their assistance and sincerest help in this work. The author is indebted to Mr. M A. Majid, Chief Scientific Officer and Head, and Mr. A. K. M. A. Hakim, Senior Engineer, Magnetic Materials Division, of Atomic Energy Centre, Dhaka, for their keen interest in the work and valuable help in the preparation of a Ni-Zn ferrite sample for this study.*

*The author feels his deepest gratitude to Dr. K. R. Rao, Head, Solid State Physics Division, and Dr. B. A. Dasannacharya, Director, Physics Group, Bhabha Atomic Research Centre ( BARC ), Bombay, India, for permitting and hosting him to work in their Neutron Scattering Laboratory for a period of one month. The author also expresses his sincere thanks to Dr. S. K. Paranjpe of the same organization for spending his valuable time to make the author familiar with the various technique of experimentation and data analysis in neutron scattering from ferrite materials which has helped greatly to carry out this work successfully. The author also wishes to take opportunity to thank Dr. R J Begum, Ex-Scientist of BARC, for her valuable suggestions and advice.*

*The author acknowledges the authority of Bangladesh Atomic Energy Commission and the authority of BUET for giving him necessary permission for carrying out this M. Phil. work in BUET and providing with the essential financial and technical support.*

*Finally, the author wants to express his thanks to his wife Mrs. Farida Yunus for keeping him free from family affairs during this work and also for her continuous cooperation and encouragement which was very much essential for successful completion of the work.*

# ABSTRACT

The present work involves two parts (i) study of the performance data of the Triple Axis Spectrometer in diffraction mode using a standard aluminium sample and ii) determination of the crystal and magnetic structures of the $Zn_{0.85}Ni_{0.15}Fe_2O_4$ ferrite system by neutron diffraction technique. A Triple axis neutron spectrometer has been installed at the 3 MW research reactor in the Atomic Energy Research Establishment, Savar, Dhaka. In the first part of this work the alignment of different axes of the spectrometer has been checked and its performance has been investigated by doing diffraction experiment with a standard aluminium sample. By checking the alignments, the zero-Bragg-angle position has been found out for Cu (002) monochromator crystal to reflect a monochromatic neutron beam of wavelength 1.24$\mathring{A}$. This beam is used as the incident neutron beam for neutron diffraction experiments. The correct zero position of the $BF_3$ detector used in the spectrometer for scanning of the diffracted beam has also been found out. Finally, the reproducibility of neutron diffraction data by the spectrometer has been tested using a standard powdered aluminium sample. Aluminium has a simple f.c.c. structure and produces a diffraction pattern with well separated and sharply defined Bragg peaks. The occurrence of such peaks in a diffraction pattern in correct angular sequence enables to verify the reproducibility of the diffraction data in a diffractometer. In the observed diffraction pattern all the Bragg peaks have been found to occur almost at the correct angular positions. The data has also been analyzed by Rietveld profile refinement program and a very good fit has been found. The lattice parameter of the specimen obtained from this analysis are also in good agreement with the values available in literature. All these signify a very good performance and reproducibility of the spectrometer.

In the second part of the work the crystal and magnetic structures of a $Zn_xNi_{1-x}Fe_2O_4$ mixed ferrite with x = 0.85 at room temperature has been determined. The reason for choosing this particular composition is that at room temperature and at higher Zn concentration such ferrites exhibit a deviation from the Neel type of ordering of their magnetic moments. This is the first neutron diffraction work of a magnetic material in Bangladesh. The experiment has been done using the above mentioned Triple axis spectrometer. The neutron diffraction data of the sample which is powdered and compressed into a pellet form has been taken at room temperature with the Triple axis spectrometer. The observed data has been analyzed by the Rietveld profile refinement program. The Ni-Zn mixed ferrite has a cubic spinel structure. The cell dimension and the oxygen coordinates depend on the distribution of cations and also on their size. The cell dimension and the oxygen parameters of the spinel structures of the ferrite have been determined very precisely through this refinement. The magnitudes and directions of the atomic moments in the individual lattice sites have also been found out carefully. A great emphasis has been given to look for the type of ordering followed by the magnetic moments in different lattice sites of this ferrite system. It has been found that the distribution of magnetic moments in the sample follows a non-collinear type of configuration at room temperature like many other mixed ferrites.

# CONTENTS

# *CHAPTER 1*

## INTRODUCTION

The Triple Axis Neutron Spectrometer (TAS) used in the present work has been installed at the piercing beam port of the 3 MW TRIGA MARK II Research Reactor in the Atomic Energy Research Establishment, Savar, Dhaka. This instrument is the first one of its kind in Bangladesh and can be used for both the elastic as well as inelastic neutron scattering experiments. It has a great impact on condensed matter research especially for metals and alloys. Using this instrument in various operational modes it is possible to determine the crystal and magnetic structure, phonon density of states molecular shape and size and many other structural and dynamical properties of matters. The installation of this spectrometer has added a new dimension in the field of condensed matter research facility in this country. The present work consists of the study of the performance data of the spectrometer and determination of the crystal and magnetic structure of a ferrite sample having composition $Zn_{0.8}Ni_{0.2}Fe_2O_4$. This is the first neutron diffraction measurement on a magnetic material in Bangladesh.

Neutron scattering has by now become a well established and valuable technique in condensed matter research. The importance of neutron scattering is due to the fact that it provides the most direct information about the structure and dynamics of the scattering system and moment distributions in magnetic materials. The application of neutron for condensed matter research has been treated in a number of standard texts [1-3]. Neutron diffraction is an elastic process of neutron scattering. It is a very powerful technique for the determination of structures of crystalline solids. The range of wavelengths covered by the thermal neutrons corresponds to the interatomic distances found in condensed matter. Thus thermal neutrons are appropriate probes for revealing the atomic arrangement of the samples over wide regions of reciprocal space. The regular periodic arrangement in crystalline solids is detected by examining the diffraction pattern produced by the

scattered neutrons. Diffracted beams are built up from the components of the neutron beam scattered by the individual atoms.

The principle of neutron diffraction is very similar to that of X-ray, but there are some important differences which are due to the differences in properties of the two radiations. Neutron scattering takes place from the nucleus which acts as a point scatterer (dimension $\sim 10^{-13}$ cm ) of the neutrons ($\lambda \sim 10^{-8}$ cm ), the scattering can be considered as s-wave scattering which is isotropic. Hence the nuclear scattering amplitude does not show any variation with angle and has no form factor dependence. On the other hand, in the case of X-rays, one has to put up with form factor problems.

The de Broglie wavelength of neutron is related to its energy by the expression:

$$\lambda = h/m_n v = h/(2m_n E)^{1/2}$$

From this relation it can be seen that a thermal neutron with energy 0.08 eV. has a wavelength of $1\mathring{A}$. The interatomic distances in most of the crystalline solids ranges from $1\mathring{A}$ to $3\mathring{A}$. Hence the wavelength of thermal neutrons is comparable to interatomic distances in condensed matter and there are significant interference effects between waves elastically or inelastically scattered from different scattering centers. The wavelengths of available useful neutrons can be varied over quite a large range to suit a desired length scale from a fraction of $\mathring{A}$ to an order of $10\mathring{A}$. The useful range of wavelengths available at the high flux reactor at ILL Grenoble, using hot and cold moderators, is for example between 0.5 - $20\mathring{A}$. The new generation spallation neutron sources can provide a particularly rich epithermal flux and a useable flux of even shorter wavelength neutrons

( 0.1 - 0.5Å ). Ultracold neutrons with wavelengths upto several hundreds of Angstroms have also been produced.

The nuclear scattering amplitude for neutrons (denoted by b ) does not depend in a systematic way on the atomic number in an atom but varies non-monotonically from one element to another. Thus b( H ) = -3.74 fm, b( He ) = 3.26 fm, b( Li ) = -2.14 fm, b ( C ) = 6.65 fm, b( O ) = 5.8 fm, b( N ) = 9.4 fm etc. Further, being a nuclear property, the scattering amplitudes may differ considerably for different isotopes of a given chemical species e. g. b( $^{1}H_{1}$ ) = -3.74 fm, b( $^{2}H_{1}$ ) = 6.67 fm etc. Hence, locations of atoms which are neighbours in the periodic tables and even neighbouring isotopes in alloys can be identified by neutron diffraction. Due to fundamental differences between the scattering process of neutron and X-rays the precise knowledge of the positional parameters of the nuclei is provided by the neutrons while X-ray amplitudes provide a measure of the charge distribution in the solids, the centroids of the charge density being considered as the positions of the atoms.

Neutrons are neutral particles and they interact with matter rather weakly. Combined with the fact that their absorption in a large majority of elements is low, they can penetrate the bulk easily. This makes neutrons a good probe for the study of bulk or volume properties of matter.

The most important and the unique advantage of neutron diffraction is that it can reveal the magnetic structures of solids. This is because the magnetic moments of neutrons interact with the magnetic moments of the atoms at different sites of the crystal lattice of a specimen. Neutrons can thus see elementary magnetic moments, whereas X-rays can not. An X-ray photon sees the

spatial distribution of electronic charge, whether or not the charge density is magnetized or unmagnetized. The cross-section for the neutron-electron interaction is of the same order of magnitude as for the neutron nuclear interaction.

The magnitude and direction of the magnetic moments of various atoms with respect to the crystal axes in solids define the magnetic structure. In a paramagnetic material the atomic moments are orientationally disordered and the scattering from such a system is incoherent. However, in an ordered ferro-, ferri- or antiferromagnet there is a regular periodicity of atomic magnetic moments in the lattice which manifests itself as Bragg peaks in a diffraction pattern. When the magnetic periodicity is the same as that of the nuclei, the magnetic Bragg peaks overlap with the nuclear peaks, while additional peaks are observed if the magnetic cell is different from the nuclear unit cell. For example, if in a b.c.c. structure the magnetic moments of the corner atoms and the body-centered atoms are parallel to each other, the nuclear and magnetic peaks will overlap, since the atomic and magnetic periodicity is the same. However, if the body-centered atom has its magnetic moment oppositely aligned with respect to that of the corner atom, the two atoms are not magnetically equivalent and additional peaks like (100), which are otherwise extinct, will appear. The structure can now be looked upon as two interpenetrating cubes displaced by ( 1/2, 1/2, 1/2 ).

Thus, diffraction of neutrons by a magnetic crystal allows the determination of the distribution, direction, and order of the magnetic moments, which one can not get from bulk magnetization measurements. Bulk magnetization measurement gives only the average magnetization of a material. Neutron diffraction is therefore, the most powerful technique to study the magnetic sublattices of ferri- and antiferromagnetic materials. C. G. Shull and et al.[4] first

determined the antiferromagnetic ordering in MnO by neutron diffraction. Since then, a number of collinear and noncollinear structures have been investigated using neutrons. The magnetic structure of Chromium has also been studied by C. G. Shull and M. K. Wilkinson[5] using the neutron diffraction technique.

Recent progress in electronics, especially in high frequency techniques, has promoted the advancement of high frequency magnetic materials technology and finally has led to the tremendous development of new homogeneous magnetic materials with high resistivity and strong magnetic properties. This requirement of high resistivity is absolutely essential at microwave frequencies, since the eddy current power loss is proportional to the square of the frequency. Snoek[6] and his collaborators of Phillips Research Laboratories in Holland undertook extensive investigations of magnetic oxides and produced a large number of ferrites of considerable commercial importance and also provided great stimulus to the experimental and theoretical work. Ferrites are ideal substance for the study of ferrimagnetism and superexchange interactions. These are extensively used at both radio and microwave frequencies and have given rise to over all improvements in communications and computer technology. They are also used as deflection yoke cores in a television picture tube, as cores of fly back transformers in television scanning, in receiving and transmitting antennas and as magnetic memories and switches. Because of these various uses of ferrites, many researchers have tried to improve their magnetic properties by looking into the structure in various ways. Neutron diffraction technique has extensively been used to explore the magnetic structures of ferrites.

The neutron diffraction observation of the distribution of magnetic moments of manganese ferrite was reported by J. M. Hastings and L. M. Corrlis[7] . The inverted spinel structure of nickel

ferrite and the normal spinel structure of zinc ferrite have also been confirmed through neutron diffraction studies by the same authors[8]. The magnetic properties of ferrites are strongly dependent on the composition and the preparation conditions. The mixed ferrites of the type $Zn_xNi_{1-x}Fe_2O_4$ has some interesting magnetic properties. These exhibit a deviation from the Neel type of ordering of their magnetic moments at room temperature. N. S. Satya Murthy et al.[9] has shown that the higher the concentration of Zn the greater is the deviation from the Neel model and these type of ferrites exhibit the Yafet-Kittel (Y-K)[10] type of noncollinear ordering of moments rather than the Neel type of collinear ordering. In this work we have done neutron diffraction of a mixed ferrite $Zn_{0.85}Ni_{0.15}Fe_2O_4$ which contains 85 molecular percent of Zn. The concentration of Zn in this ferrite specimen is thus very high Such a composition has been chosen with an objective to look for the Y-K type of ordering of magnetic moments. At lower concentration of Zn, the ordering of magnetic moment is of Neel type and the moments on each site can be measured by other methods and even it can be estimated easily from the composition But for Y-K type of ordering the moments in B site can not be estimated unless the Y-K angle is known. So, for this composition, one needs to do neutron diffraction measurements of the specimen to determine the correct magnetic structure. As the time required for a neutron diffraction experiment is very long, it has not been possible to study the other composition with lower concentration of Zn. The crystal and magnetic structure of the sample at room temperature have been studied by Rietveld profile refinement of the neutron diffraction data. Efforts have been made to determine the magnitudes and directions of the atomic moments on the individual lattice sites with great emphasis to look for the type of ordering it follows. The existence of Y-K type of ordering has been confirmed for this specimen through this study.

# *CHAPTER 2*

## *THEORY*

Neutrons interact weakly with matter, the scattering can be satisfactorily treated within first Born approximation. One can derive general expressions for the scattering cross-section without first going into the explicit form of the interaction potential. It may be noted, however, that the interaction potential has two major parts, which form the basis of most neutron scattering investigations. The first is the interaction of neutrons with the nuclei of the target via nuclear forces. This gives rise to what is commonly termed as nuclear scattering. This interaction is in general nuclear and neutron spin dependent. Further, neutron has a half integral spin and a magnetic moment = -1.91 nuclear magnetons. The second major part is the electromagnetic interaction between the magnetic moment of neutron and that of the magnetic or unpaired electrons in the scatterer. The scattering due to this interaction is referred to as magnetic scattering.

The scattering of neutrons has a great deal of similarity and complementary to other radiations used for studying condensed matter, like photons ( light, X-rays ) or electrons, due to the common wave aspect in all the cases and despite the quantitative differences due to the different nature of interactions[2] . The range of wavelengths of thermal neutrons corresponds to the interatomic distances found in condensed matter. Thermal neutrons, X-rays and electrons are suited for study of condensed matter but in the study of magnetic moment distributions and magnetic excitations, the role of neutrons is quite unique. It has been seen that the amplitude for nuclear scattering from nuclei is of order $10^{-12}$cm. In favourable cases the magnetic scattering amplitude from atomic moments can also be of the same order of magnitude. The energy of thermal neutrons is also of same order as the energy of many low lying excitations like phonons,

magnons or molecular motions. With a proper choice of incident energy the neutrons can exchange a comparable fraction of their own energy during scattering, making them a sensitive spectroscopic probe.

## 2.1 SCATTERING FROM A PERIODIC LATTICE:

To consider the scattering from a periodic crystal lattice, the scattering potential appropriate for isotropic scattering in Born approximation is best represented by the Fermi pseudo-potential

$$V(\underline{r}) = 2\pi\hbar^2/m \, .b \, . \, \delta \, ( \underline{r} - \underline{R} )$$

where $\underline{R}$ is the position of the nucleus with neutron scattering length b. For an array of nuclei at $R_j$ having scattering amplitudes $b_j$

$$V(\underline{r}) = 2\pi\hbar^2 /m \, \Sigma_j \, b_j \, \delta \, ( \underline{r} - \underline{R}_j )$$

with this $V(\underline{r})$, the master formula for the scattering cross-section is

$$\partial^2\sigma/\partial\Omega\partial E = \underline{k}'/k \, \Sigma_{A,\sigma} p_A p_\sigma \, \Sigma_{A'\sigma'} \, |\langle \sigma' A' | \Sigma_j \, b_j \exp\left(i\underline{\chi}.\underline{R}_j\right) \sigma A\rangle|^2 \delta\left(\hbar\omega + E_A + E_{A'}\right) \quad .. \; .. \; .. \; .. \; (1)$$

For elastic scattering, $d\sigma/d\Omega$ will be

$$d\sigma/d\Omega = \Sigma_{A,\sigma} \, p_A p_\sigma \, \Sigma_{jj'} \exp\left\{ i\underline{\chi}.\left(\underline{R}_j - \underline{R}'_j\right) \right\} \langle \sigma A | b^*_{j'} b_j | \sigma A \rangle$$

$$= \Sigma_{jj'} \exp\left\{ i\underline{\chi}.\left(\underline{R}_j - \underline{R}_{j'}\right) \right\} \overline{b^*_{j'} b_j}$$

where $|\overline{b^*_{j'} b_j}| = \Sigma p_A \langle A | b_{j'} b_j | A \rangle$

$|\overline{b^*_{j'} b_j}| = \overline{b^*_{j'}}\,\overline{b_j} = |\overline{b}|^2$ for $j \neq j'$

$= |\overline{b_j}|^2 = \overline{|b|^2}$ for $j = j'$

Therefore, in general we can write

$$\overline{b_j^* b_{j'}} = |\bar{b}|^2 + \delta_{jj'}\left(\overline{|b|^2} - |\bar{b}|^2\right)$$

The expression for $d\sigma/d\Omega$ contains information about both the coherent and incoherent scattering i. e.

$$d\sigma/d\Omega = \left(d\sigma/d\Omega\right)_{coh.} + \left(d\sigma/d\Omega\right)_{incoh.}$$

where

$$\left(d\sigma/d\Omega\right)_{coh.} = |\Sigma_j b_j \exp\left(i\underline{\chi}.\underline{R_j}\right)|^2$$

and

$$\left(d\sigma/d\Omega\right)_{incoh.} = \left\{\overline{|b|^2} - |\bar{b}|^2\right\}$$

The coherent scattering cross-section is a maximum for $\chi = 0$ or $\chi$ = any point in reciprocal lattice i.e.

$$\left(d\sigma/d\Omega\right)_{coh.} = N\frac{(2\pi)^3}{v_0}\Sigma_{\underline{G}}\,\delta\left(\underline{\chi} - \underline{G}\right)|F_N\left(\underline{G}\right)|^2$$

which is in fact, the Bragg reflection condition for $\underline{G}$ . Where $\underline{G}$ is the reciprocal lattice vector , N is the number of unit cell in the sample and $v_0$ is the volume of the unit cell. In this expression F ($\underline{G}$) is

$$F_N\left(\underline{G}\right) = \Sigma_j b_j \exp\left(2\pi i\underline{G}.\underline{R_j}\right)$$

## 2.2 BRAGG SCATTERING:

The diffraction of X-rays or neutrons are governed by the Bragg law

$$n\lambda = 2d\sin\theta$$

where n is an integer called the order of reflection , d is the spacing of the atomic planes in the crystal and $\theta$ is the angle between the incident beam and the atomic planes involved. When the neutrons or X-rays encounter an atom , they are scattered in all directions, and what we call a diffracted beam is simply a set of scattered beams which are in phase, so that they reinforce one another. The Bragg condition is that the rays scattered in the directions making an angle $\theta$ with the atomic planes equal to the angle of incidence will be in phase with one another. In all other directions of space the phase relations between the scattered beams are such that they cancel one another. In experimental work, the angle $2\theta$, rather than $\theta$, is usually measured; it is the angle between the diffracted beam and the transmitted beam.

Scattering from a polycrystalline or powdered sample takes place into Debye-Scherrer cones with the incident $\underline{k}$ direction as axis and semiangle $2\theta$. Then the total cross-section associated with each cone is

$$\sigma(hkl) = \frac{4\pi^3}{k^2}\frac{N}{v_0}\frac{j}{4\pi\sin\theta/\lambda}|F_N(\underline{G})|^2$$

where j is the multiplicity of the reflection ( h k l). The counter observes only a fraction ($l/2\pi r\sin 2\theta$) of the complete cone where

l = the height of the counter

r = sample to counter distance.

If $I_0$ is the initial intensity, the intensity of the diffracted beam I is thus

$$I = I_0 (\lambda^3 l/8\pi r)(vjN_c^2|F(\underline{G})|^2)/(\sin\theta \sin 2\theta)$$

where v is the volume of the sample and $N_c$ is the number of unit cells per unit volume.

For a polycrystalline sample with a vertical circular cylindrical shape , the expression for the experimental intensity can be written as:

$$I = I_0 [(\lambda^3 l/8\pi r)(vjN_c^2|F(\underline{G})|^2)/(\sin\theta \sin 2\theta)]\frac{\rho'}{\rho} A_{hkl} e^{-2W} \quad .. \quad .. \quad .. \quad (2)$$

where $\rho'$ = measured density of the specimen,

$\rho$ = theoretical density,

$e^{-2W}$ = Debye temperature correction factor,

$A_{hkl}$ = absorption factor.

## 2.3 MAGNETIC SCATTERING:

Neutrons possess a magnetic moment and are scattered from magnetic moments associated with the unpaired electrons in atoms. The magnetic scattering amplitude of the neutron has an angular dependance called the magnetic form factor. The occurrence of this form factor determining the magnetic scattering, in contrast to the absence of any such factor for the nuclear scattering, arises since the electrons which determine the magnetic moment will be distributed over

a volume of space having linear dimensions comparable with the neutron wavelength. Thus this form factor is somewhat similar to the electronic form factor of an atom for X-ray scattering, although the two are by no means identical since it is only a few electron orbits in an outer shell of the atom which contribute to the magnetic moment and, hence, to the form factor for the magnetic scattering of neutrons. It is found , indeed that the form factor for magnetic neutron scattering falls off more rapidly with angle than does the factor for X-ray scattering. Magnetic scattering arising from the interaction of neutron magnetic moment with the atomic moments is given by

$$V_m(\underline{r}, t) = -\underline{\mu}_n \cdot \underline{M}(\underline{r}, t)$$

where $\underline{M}(\underline{r}, t)$ is the magnetic moment density and $\underline{\mu}_n$ is the neutron magnetic moment.

## Paramagnets:

In the case of para magnetic material with no external magnetic field, the atomic magnetic moments are randomly oriented with respect to each other and there is no spatial correlation between them. For such a system the scattering from a single atom is given by

$$d\sigma/d\Omega \propto (e^2\gamma/m_e c^2)^2 f^2(\underline{Q}) \tfrac{2}{3} S(S+1)$$

where S is the atomic spin and f ( Q ) is the magnetic form factor. Since there is no long range magnetic order in paramagnetic materials there is no Bragg reflection from magnetic scattering. For magnetically disordered systems (paramagnetic materials) the scattering will be incoherent and

due to the form factor term, it will fall as a function of scattering angle. The nuclear periodicity is shown by well defined Bragg peaks and the magnetic scattering contributes to background which shows the $f(\underline{Q})$ dependence.

## Magnetically ordered system:

For magnetically ordered materials the scattering cross-section has been worked out by Halpern and Johnson for spin only moment. The coherent scattering amplitude for an atom with non-zero magnetic moment is given by

$$b + (\underline{q} \cdot \underline{\lambda}) p$$

where $\underline{\lambda}$ is the unit neutron polarization vector and q is the magnetic interaction vector defined as

$$\underline{q} = \underline{e}(\underline{e} \cdot \underline{s}) - \underline{s}$$

where $\underline{e} = (\underline{k} - \underline{k}')/|\underline{k} - \underline{k}'|$ and $\underline{s}$ is the unit vector in the direction of the magnetic moment of the atom. The symbol p represents the magnetic scattering amplitude and for spin only case it is given as

$$p = (e^2 \gamma_n / m_e c^2) S f$$
$$= 0.54 S f \times 10^{-12} cm$$

So, the magnitude of p is comparable with that of the nuclear scattering length b. This scattering amplitude is the magnetic counterpart of the nuclear scattering amplitude b and gives rise to the build up of coherent diffraction peaks dependent on the three dimensional magnetic structure of a domain, which will be the counterpart of the crystallite for ordinary nuclear scattering. The expression for p can be rewritten as

$$p = (e^2 \gamma / 2 m_e c^2) 2Sf$$

containing the factor 2S which for an atom in which the orbital moment is completely quenched, is equal to the magnetic moment expressed in Bohr magnetons. For an atom in which both spin and orbital moments are operative we merely replace 2S by the corresponding value of the magnetic moment ,namely, gj, where g is the Lande splitting factor. Thus, in general case we have

$$p = ( e^2 \gamma/2m_e c^2 ) gjf$$

The differential scattering cross-section for magnetic atom is then given by

$$d\sigma/d\Omega \propto b^2 + q^2p^2 + 2bp\underline{q}.\underline{\lambda}$$

For unpolarized neutron case the term $\underline{q}.\underline{\lambda}$ averages out to zero and

$$d\sigma/d\Omega \propto b^2 + q^2p^2$$

For an array of atoms in a periodic lattice the total scattering amplitude is replaced by the unit cell structure factor F ( $\underline{G}$ ) i. e.

$$F(\underline{G}) = \Sigma_j \left(b_j + q_j p_j\right) \exp i\left(\underline{G}.\underline{R}_j\right)$$

The scattering cross-section is then written as

$$d\sigma/d\Omega \propto F_N^2 + q^2F_M^2$$

where $F_M$ is the magnetic structure factor defined analogous to nuclear structure factor as

$$F_M = \Sigma_j q_j p_j \exp i\left(\underline{G}.\underline{R}_j\right)$$

For collinear structures atomic moments $q_j$ is same for all the atoms and can be taken out of summation , but in general cases where the moments at two sites have relative orientation, like in helical structures, q is site dependent. $q^2$ can be written as

$$q^2 = e^2 (\underline{e} \cdot \underline{s})^2 + s^2 + 2 (\underline{e} \cdot \underline{s})^2$$

$$= 1 - (\underline{e} \cdot \underline{s})^2$$

$$= 1 - (\cos^2 \alpha)$$

$$= \sin^2 \alpha$$

where $\alpha$ is the angle between the scattering and magnetization vector.

Thus in the expression for scattering cross-section the magnetic interaction vector provides information about the relative orientations of the atomic magnetic moments. In the case of diffraction of unpolarized neutrons from unmagnetized sample $q^2$ is the average over the orientations and for a cubic system it is 2/3.

## 2.4 CRYSTAL STRUCTURE OF FERRITES:

Magnetite, $Fe_3O_4$ is the first magnetic substance known to people and it was being used by the ancient navigators in their compasses. The term ferrite denotes a group of iron oxides of which $Fe_3O_4$ is a typical one. Ferrites are said to have the cubic structure very close to that of the mineral spinel $MgO.Al_2O_3$ and are called cubic spinels. Formerly, spinels containing Fe were called ferrites, but now the term has been broadened to include many other ferrimagnets including garnets and hexagonal ferrites and these need not necessarily contain iron. The general chemical

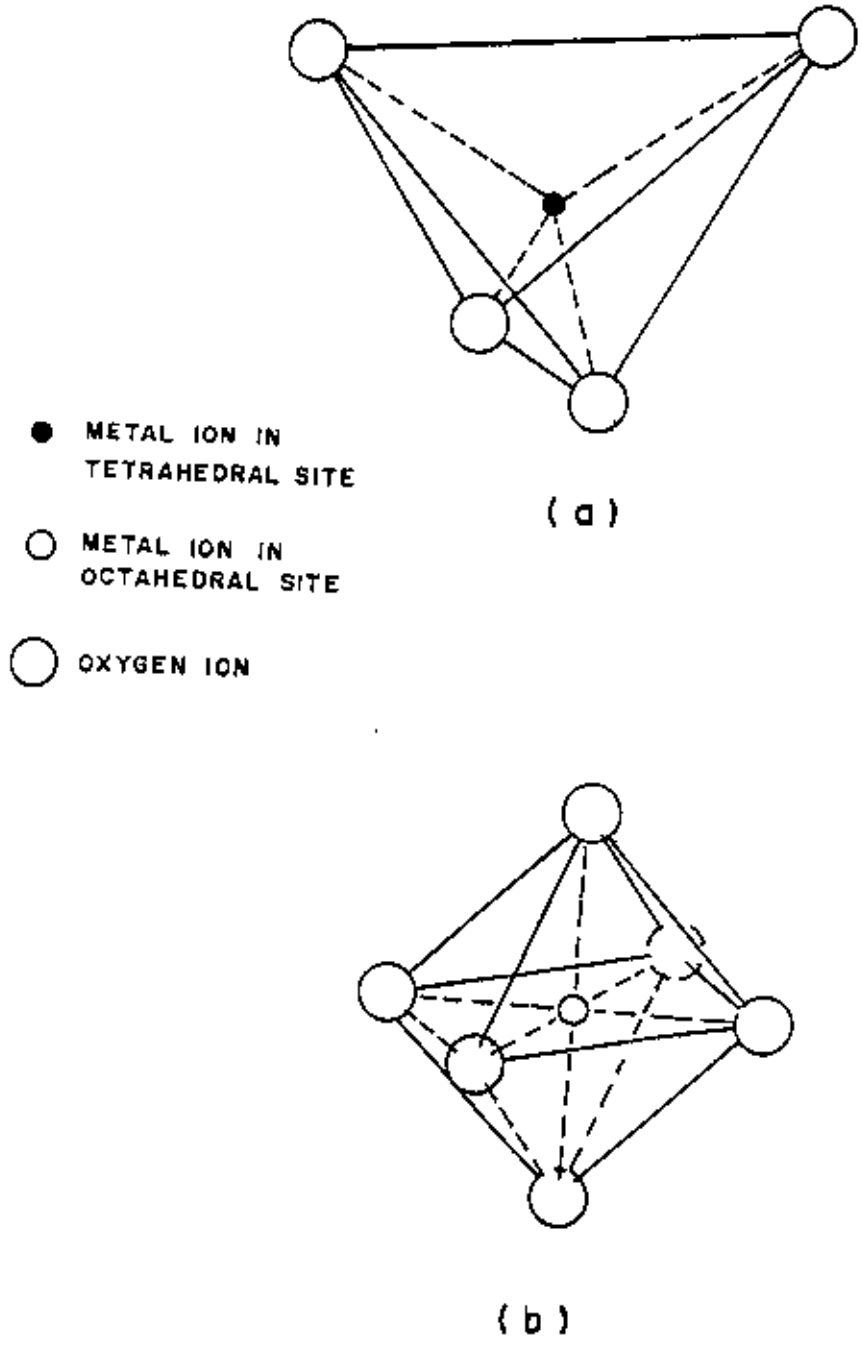


**Fig. 2.1 ( a ) Tetrahedral A Site, ( b ) Octahedral B Site.**

formula is $AB_2X_4$ where A and B represent metal ions and X is oxygen in a great majority of the cases. but may also be sulphur, selenium or fluorine. The spinel structure is complex in that there are 8 molecules or a total of 8 x 7 = 56 ions per unit cell. The frame work of spinel structure is the lattice of anions which has a close packed f.c.c. array. The metal ions which are much smaller in dimensions fit into the interstices of the anion lattice. There are two kinds of interstices. One is called the A site which has the tetrahedral coordination of anions ( Fig.2.1a ) and the other is called the B site having an octahedral coordination ( Fig.2.1b ). In all there are 64 A sites and 32 B sites of which only 8 and 16 respectively are occupied in a spinel

The unit cell contain so many ions that a drawing of the complete cell would not be informative. Instead we can imagine the unit cell of edge $a_0$ to be divided into eight octants each of edge $a_0/2$ as shown in Fig.2.2a. The four shaded octants have identical contents and so do the four unshaded octants. The contents of the two lower-left octants in Fig.2.2a are shown in Fig.2.2b. One tetrahedral site occurs at the corner of the right octant of Fig.2.2b, and other tetrahedral sites are at certain octant corners. Four octahedral sites occur in the left octant; one is delineated by dashed lines to six oxygen ions, two of which, shown dotted, are in adjacent octants behind and below. Oxygen ions are represented by large spheres and small black spheres and small white spheres represent the metal ions in A and B sites respectively. The oxygen positions are the same (tetrahedrally arranged) in all the octants but the metal ions are identical only in octants sharing a common edge or corner and are different in octants having a common face. The rest of the unit cell can be constructed by successive translations along the three [110] axes. The A site ions form two interpenetrating f.c.c. lattices having an edge $a_0$ which are displaced with respect to each other over a distance $1/4a_0\sqrt{3}$ in the [111] direction that is along the body diagonal.

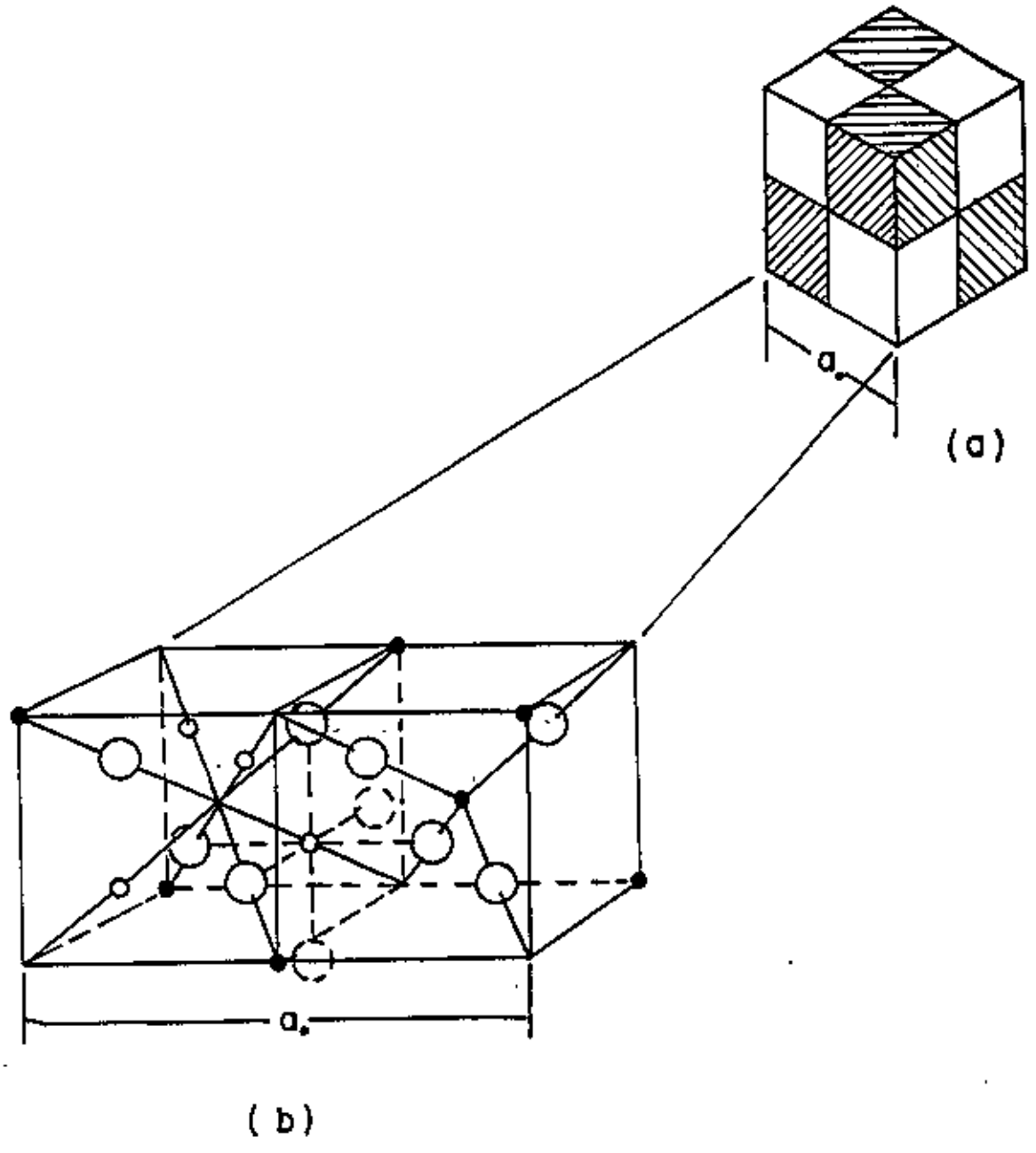


**Fig. 2.2 Crystal Structure of a Cubic Ferrite.**

The B site ions constitute four interpenetrating f.c.c. lattices that are displaced with respect to each other by a distance of $1/4a_o\sqrt{2}$ along [110] direction that is along the face diagonals.

The spinel structure belongs to the space group $Fd3m(O^7_h)$ and in the centrosymmetric representation the ionic positions in the unit cell are given by

A site ions (8a): (1/8,1/8,1/8); (7/8,7/8,7/8); F.C.

B site ions (16d): (1/2.1/2,1/2); (1/2,1/4,1/4): (1/4,1/2,1/4):
(1/4,1/4,1/2); F.C.

Oxygen ions (32e): ±(u,u,u); (u,1/4-u,1/4-u); (1/4-u,u,1/4-u); (1/4-u,1/4-u,u); F.C.

When u = 0.25 exactly the oxygen ions form a cubic close packed array; otherwise it is approximately so. In reality, there is always some deviations from the ideal value caused by the cations. The radii of the A and B site on a hard sphere model are given by

$$r_a = ( u - 1/8 )a_o\, 3 - R_o$$

and $$r_b = ( 1/2 - u )a_o - R_o$$

where $R_o$ is the radius of oxygen ion, $O^{2-}$. In most of the ferrites the A sites have relatively smaller dimensions than the B sites and in general too small to accommodate a cation without local

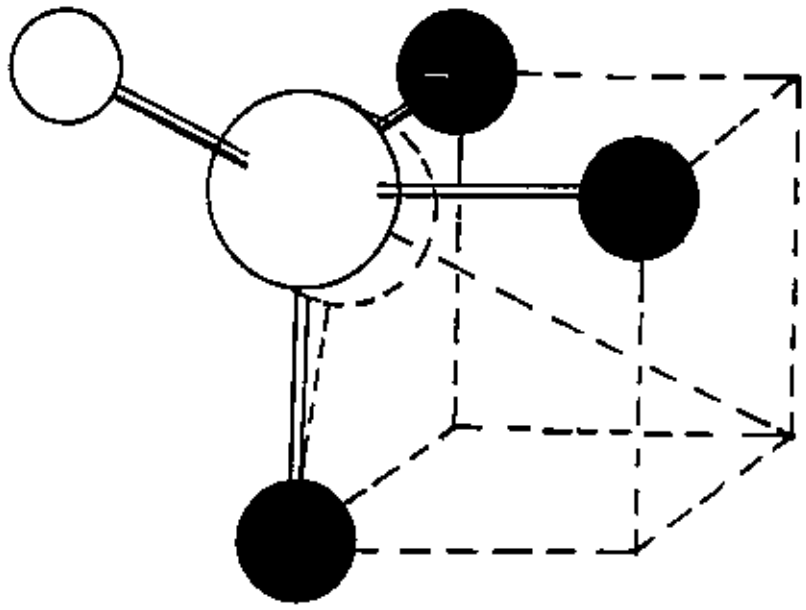

Fig. 2.3 Distortion of the Spinel Lattice as a result of the non-ideal value of the Oxygen Parameter, u.

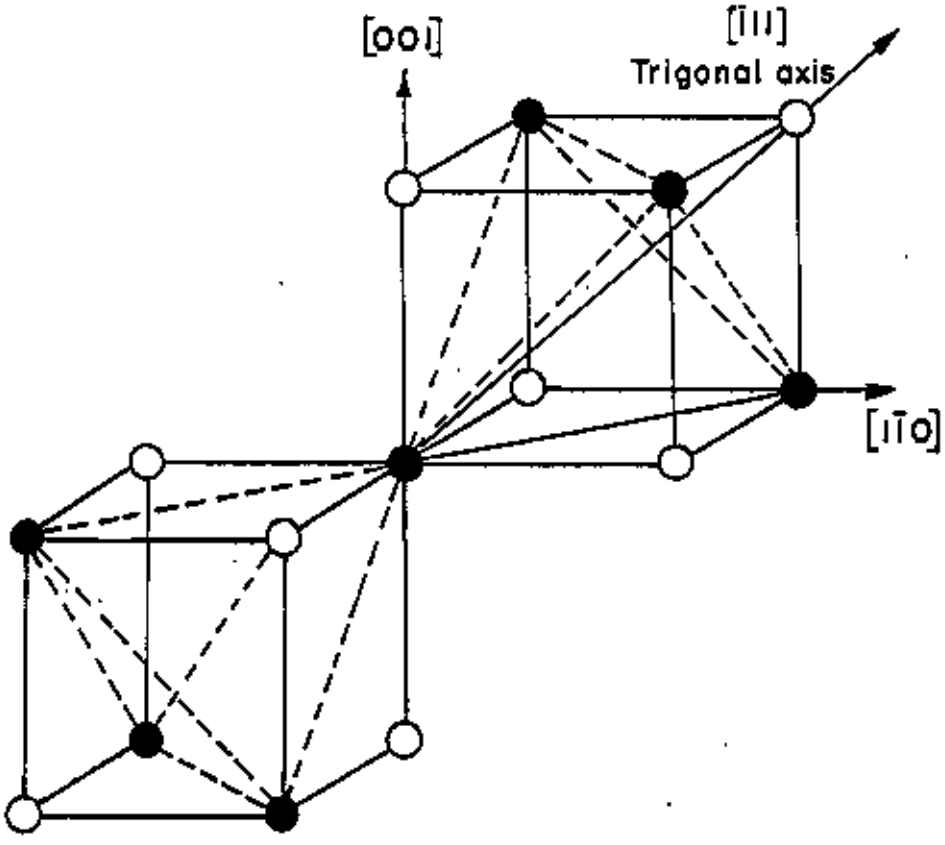


**Fig. 2.4 Symmetry around the B Site of a Spinel Lattice.**

distortion of the site or the ion. An expansion of these sites takes place as shown in Fig.2.3 by displacing the nearest neighbour oxygen ions along the body diagonal of the cube. Hence, any u parameter greater than 0.25 implies an expansion of the oxygen lattice around the A sites and a corresponding contraction about B sites. However, the symmetry around an A site is strictly cubic even if u is not equal to 0.25 because the oxygen ions still form a tetrahedron. The B site cations have a cubic coordination of oxygen ions in the ideal case of u =0.25, but the 6 next nearest neighbour cations belonging to other B sites have trigonal symmetry around one of the [ 111 ] directions, as shown in Fig2.4. Since all the [ 111 ]directions have equal probability of being symmetry axes, the overall symmetry of the B site cation is also cubic in ideal case. But when u is not equal to 0.25, the symmetry no longer remains cubic, but gets lowered to that of the neighbouring B cations. It should also be noted that the deviation from the ideal lattice introduce a trigonal field component due to the oxygen ions also. However, the axis of this anion crystalline field coincides with that due to the cation sublattice and no new crystal field symmetries are introduced. This trigonal field plays an important role in the magnetostriction and magnetocrystalline anisotropy of certain spinels.

## Cation Distribution:

A large family of ferrites having the general formula $MFe_2O_4$ may be derived from $Fe_2O_4$ by replacing the diavalent iron by one or more diavalent cations ( M ), provided their ionic radii are comparable to that of $Fe^{2+}$. The cations can be distributed over the two possible sites A and B in a

variety of ways and the two extreme cases are known as "normal" and "inverse" ferrites. In general, $Fe^{3+}$ ions may be present on both the sites. Let the proportion of iron on A and B sites be $\lambda:\mu$, where $\lambda + \mu = 1$.

i) When $\lambda = 0$, the A sites are occupied by only $M^{2+}$ ions and the structure is said to be normal.

ii) In an inverted structure $\lambda = \mu = 0.5$, so that $Fe^{3+}$ ions are equally distributed among the two sites and all $M^{2+}$ ions are on the B sites.

Many ferrites have cation distributions that are intermediate between these extremes The basic magnetic properties of the ferrites are very sensitive functions of their cation distribution. Mixed ferrites having interesting and useful magnetic properties are prepared by mixing two or more kinds of metal ions M.

When the cations have appreciably different magnetic moments their distribution can be obtained from saturation magnetization measurements extrapolated to 0°K. X-ray diffraction has also been used to determine the distribution, but ions of neighboring atomic numbers are difficult to distinguish by this means and in such cases neutron diffraction proves to be an extremely powerful tool.

## 2.5 MAGNETISM IN FERRITES:

The magnetism exhibited by ferrites falls under the category of ferrimagnetism. Actually, ferrimagnetism was postulated by Neel[11] to account for the behavior of ferrites. He achieved considerable success in interpreting the magnetic properties of a large number of ferrites in terms of his simple and elegant theory although there are few exceptions.

Ferrimagnetism may be considered as an special case of antiferromagnetism or perhaps vice versa, because in this case at least two unequal and antiparallel systems of atomic moments exist giving rise to a resultant spontaneous magnetic moment. The simplest case is that of a two sublattice system. The individual sublattice moments are aligned ferromagnetically, but the moment direction in one sublattice is opposite to that in the other. But the term "ferrimagnetism" includes materials with more than two sublattices with other complicated moment configurations. These configurations result when intrasublattice interactions become comparable with intersublattice iteractions.

The intense, short range electrostatic field which is responsible for the magnetic ordering are quantum mechanical in origin and is related to the overlap of the charge distributions of the atoms concerned. The exchange interactions coupling the spins of a pair of electrons is proportional to the scalar product of their spin vectors,

$$V_{ij} = -2J_{ij}S_i.S_j \quad .. \quad .. \quad .. \quad .. \quad .. \quad (3)$$

where $J_{ij}$ is the exchange integral given in a self explanatory notation by

$$J_{ij} = \int \Psi_i^*(1)\Psi_j^*(2)\left[\frac{2}{r_{12}} + \frac{2}{r_{ij}} - \frac{1}{r_{i1}} - \frac{1}{r_{j2}} - \frac{1}{r_{i2}} - \frac{1}{r_{j1}}\right] \times \Psi_i(2)\Psi_j(1)d\nu_1 d\nu_2 \quad .. \quad .. \quad .. \quad .. \quad (4)$$

In this expression r's are the distances, subscripts i and j refer to the atoms, 1 and 2 refer to the two electrons.

Magnetic interactions in spinels as well as in some ionic compounds are different from one considered above because the cations are at a large distance and always have anions as nearest neighbours. These anions obscure the direct overlap of the cation charge distributions, some times partially and at times completely. Still there seems to be strong magnetic interactions present as indicated by the values of the magnetic transition temperatures. Moreover, the ratio of the distance between the ions to the diameter of the concerned electron orbits is of the order of 2.5 that is a moderate to weak positive interaction is expected[12-14] but experimental evidence are in favour of a strong negative interaction. So it is unlikely that the magnetic interactions in such structures depend on direct coupling of the cation spins. Further, the anions have zero net spins and that rules out their direct exchange interaction with neighbouring cations. A "superexchange" mechanism between cations that operate via the intermediate anions was proposed by Kramer[15] for such cases and was developed by Anderson[16] and Van vleck[17]

A simple example of superexchange is provided by MnO which was chosen by Anderson. Its ground state electronic configuration can be written as

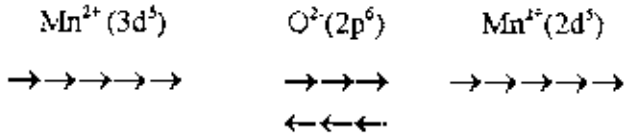

In this state there can not be any spin coupling of the oxygen (g = 0) with the cations. Now let the oxygen be in an excited state when one p electron leaves the oxygen ion and becomes temporarily a part of one of the Mn ions. The new configuration will be

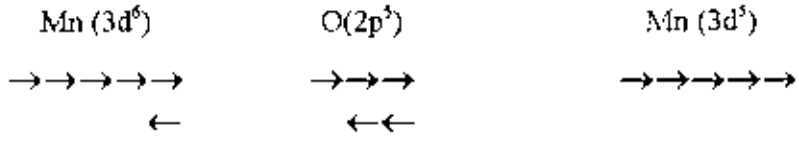


The resulting spin of the oxygen ion can now have a direct exchange interaction with the other Mn ion. If the separation between them is not very large the interaction will be negative and as a result the two Mn ions will have antiparallel spins.

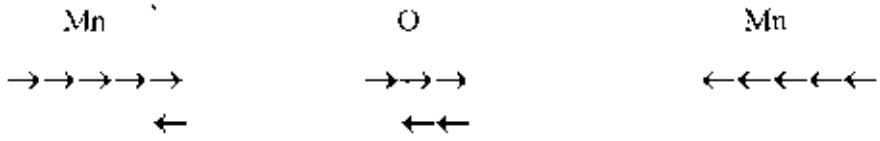


In the case of spinel ferrites also the coupling is of the indirect type involving overlap of oxygen wave functions with those of the neighbouring cations. The essential point is that when an oxygen p orbital overlaps a cation d orbital one of the p electrons can be accepted by the cations. This p electron will go into the next available place in the 3d shell according to Hund's rule, so that if the cation concerned has less than half-filled 3d shell the spin of the transferred electron will be parallel to the net spin of the cation, but it will be antiparallel if the 3d shell is at least half-filled. When the two cations are identical, they must have opposite net spins in order to fulfil Hund's rule

for both the ions, since the two p electrons of the oxygen must have antiparallel spins by the Pauli exclusion principle.

## The Neel theory of Ferrimagnetism:

Let us consider the simplest case of a two sublattice system having antiparallel and non-equal magnetic moments. The inequality may be due to

i) different elements in different sites,

ii) same element in different ionic states,

iii) different crystalline fields leading to different effective moments for ions having the same spin.

The spins on one sublattice are under the influence of exchange forces due to the spins on the second sublattice as well as due to other spins on the same sublattice. The molecular fields acting on the two sublattices A and B can be written as

$$H_A = \lambda_{AA} \; M_A + \lambda_{AB} \; M_B$$

$$H_B = \lambda_{BA} \; M_A + \lambda_{BB} \; M_B$$

where $M_A$ and $M_B$ are the magnetizations of the two sublattices and $\lambda$'s are the Weiss constants. Since the interaction between the sublattices is antiferromagnetic $\lambda_{AB}$ must be negative, but $\lambda_{AA}$ and $\lambda_{BB}$ may be negative or positive depending on the crystal structure and nature of the interacting atoms. Probably, these interactions are also negative, though in general quite small

Assuming all the exchange interactions to be negative the molecular fields will be given by

$$H_A = -\lambda_{AA} M_A - \lambda_{AB} M_B$$

$$H_B = -\lambda_{AB} M_A - \lambda_{BB} M_B$$

Since in general, $\lambda_{AA}$ and $\lambda_{BB}$ are small compared to $\lambda_{AB}$, it is convenient to express the strengths of these interactions relative to the dominant $\lambda_{AB}$ interaction.

Let $\lambda_{AA} = \alpha\lambda_{AB}$

and $\lambda_{BB} = \beta\lambda_{AB}$

In an external applied field $H$, the fields acting on A and B sites are

$$H_A = H - \lambda_{AB}(\alpha M_A - M_B)$$

$$H_B = H - \lambda_{AB}(M_A - \beta M_B)$$

At temperatures higher than the transition temperature, $T_N$, $H_A$, $M_A$ and $M_B$ are all parallel and we can write

$$\underline{M}_A = \frac{C_A}{T}[\underline{H} - \lambda_{AB}(\alpha\underline{M}_A - \underline{M}_B)]$$
$$\underline{M}_B = \frac{C_B}{T}[\underline{H} - \lambda_{AB}(\underline{M}_A - \beta\underline{M}_B)] \quad \ldots\ \ldots\ \ldots\ (a)$$

where $C_A$ and $C_B$ are the Curie constants for the two sublattices.

$$C_A = N_A g\mu_B^2 S_A(S_A + 1)/3K$$

and $$C_B = N_B g\mu_B^2 S_B(S_B + 1)/3K$$

$N_A$ and $N_B$ denote the number of magnetic ions on A and B sites respectively and $S_A$ and $S_B$ are their spin quantum numbers. Solving for the susceptibility, $\chi$, one gets

$$\frac{1}{\chi} = \frac{T}{C} - \frac{1}{\chi_0} - \frac{\sigma}{T-\theta'} \quad \ldots\ \ldots\ \ldots\ (b)$$

where C, $\chi_0$ and $\theta'$ are constants for a particular substance and are given by

$$C = C_A + C_B$$

$$\frac{1}{\chi_0} = -\frac{1}{C^2}[C_A^2\lambda_{AA} + C_B^2\lambda_{BB} + 2C_AC_B\lambda_{AB}]$$

$$\sigma = \frac{C_AC_B}{C^3}[C_A^2(\lambda_{AA} - \lambda_{AB})^2 + C_B^2(\lambda_{BB} - \lambda_{AB})^2$$

$$-2C_AC_B\{\lambda_{AB}^2 - (\lambda_{AA} + \lambda_{BB})\lambda_{AB} + \lambda_{AA}\lambda_{BB}\}]$$

$$\theta' = -\frac{C_AC_B}{C}(\lambda_{AB} + \lambda_{BB}) - 2\lambda_{AB}$$

The equation ( b ) for $\frac{1}{\chi}$ is a hyperbola and is the characteristic which differentiates ferrimagnets from ferromagnets.

The ferrimagnetic Neel temperature, $T_N$, is obtained from equation ( a ) with H = 0 and setting the determinant of the coefficients of $M_i$ equal to zero. This gives

$$T_N = -\frac{1}{2}[C_A\lambda_{AA} + C_B\lambda_{BB} + \frac{1}{2}\{(C_A\lambda_{AA} - C_B\lambda_{BB})^2 + 4C_AC_B\lambda_{AB}^2\}^{\frac{1}{2}}]$$

The sublattice magnetizations will in general have different temperature dependances because the effective molecular fields acting on them are different. This suggests the possibility of having anomalous net magnetization versus temperature curves. For most ferrimagnets the curve is similar to that of ferromagnets, but in a few cases there may be a compensation point or a maximum in the curve.

In an ideal inverse structure, there are equal number of $Fe^{3+}$ ions on A and B sites. So, the net magnetic moment is entirely due to $M^{2+}$ions on B sites and as such can not exceed $5\mu_B$. However, the net moment may be increased by adding a normal ferrite in which $M^{2+}$is a diamagnetic ion. In a mixed Ni-Zn ferrite when a fraction of $NiFe_2O_4$ is substituted by $ZnFe_2O_4$, the magnetic behavior shows unequivocally that $Zn^{2+}$ goes into the A site forcing a $Fe^{3+}$ ion over into a B site, thus giving rise to an additional magnetism. In a mixed ferrite system $Zn_xNi_{1-x}Fe_2O_4$, the ionic distribution may be written as

$$\left(Zn_x^{2+}Fe_{1-x}^{3+}\right)\left[Ni_{1-x}^{2+}Fe_{1+x}^{3+}\right]O_4$$

The net magnetic moment per molecule is then

$$M = [5\ (1+x) + 2\ (1-x) - 5\ (1-x)]\mu_B$$

$$= (2+8x)\mu_B$$

which is higher than that of $NiFe_2O_4$ . In general for a ferrite which consists partly of magnetic ions and partly of non-magnetic ions, the net magnetic moment will be given by

$$M = [n - (10 - n)\ x\ ]\ \mu_B$$

where n = No. of unpaired electrons of the magnetic ions and

x = Concentration of non-magnetic ions.

So M should increase from $n\mu_B$ towards 10 $\mu_B$ with additions of non-magnetic ions. Although such an increase is observed in ferrites, the full increase is not realized in practice because the dilution of magnetic ions on A sites weakens the antiferromagnetic AB interactions as can be seen from the decreasing Neel temperatures and this leads to departures from the Neel model.

Though the simple Neel theory successfully explains the observed magnetic moments and temperature dependances of the magnetization of large number of ferrites, it fails for certain cases.

i) The essential requisite for Neel configuration is a strong negative exchange interaction between A and B sublattices which results in their being magnetized in opposite directions below the transition point. But there may be cases where intrasublattice interactions are comparable with intersublattice interaction. Neel's theory predicts paramagnetism for such substances at all

temperatures. This is unreasonable since strong AA or BB interaction may lead to some kind of ordering especially at low temperature. In the cases of no AB interaction, antiferromagnetic ordering may be expected either in the A or in the B sublattice.

ii) The spontaneous magnetization of a number of ferrites is significantly lower than predicted by the Neel theory.

## Yafet-Kittel theory of ferrimagnetism:

The problem of determining the ground state spin configuration in spinels has been of considerable theoretical interest for years. Yafet and Kittel[10] were the first to overcome the difficulties encountered in the simple Neel theory by considering further subdivisions of A and B sublattices and assuming non-collinear magnetic moment arrangements. They predicted a triangular spin structure among other possibilities. When there is a strong antiferromagnetic interaction among the ions on the B sites, the magnetic moments associated with these will split into sublattices of tilted spin in response to their tendency to be simultaneously antiparallel to both their A site and B site neighbours. In the simplest case the B site cations will form two sublattices in each of which the moments are parallel but the moments in one make an angle with the moments in the other sublattice. The resultant B site moment is antiparallel to the A site moment.

Such an arrangement can explain beautifully the observed low moments in some ferrites like Zn-Ni and Zn-Mn ferrite systems.

The Yafet-Kittel (Y-K) theory of triangular moment configurations has been developed by Lotgering [118] who applied it to explain the magnetic behaviour of certain chromites. The discussion below follows his treatment.

Yafet and Kittel divided the A and B sublattices further into equivalent sublattices to take into account of different magnetic orderings allowed by the crystal symmetry of the spinel structure. On such a basis there are two A sublattices and four B sublattices. But, as shown by Yafet and Kittel, the four B sublattices may be lumped together to form two non-equivalent sublattices if anisotropy is neglected.

To determine the ground state let us assume that only one type of magnetic ion is present, though the case of several types of magnetic ions may be treated in an equivalent way. Let $\underline{M}_{a_2}$ and $\underline{M}_{b_1}$ be the magnetization vectors of the sublattices $A_1$ and $B_1$ and $\underline{M}_A$ and $\underline{M}_B$ are the resultant magnetizations of A and B lattices respectively i. e.

$$\underline{M}_A = \Sigma \underline{M}_{a_1} \quad \text{and} \quad \underline{M}_B = \Sigma \underline{M}_{b_1}$$

The molecular fields acting on the individual sublattices are

$$\underline{H}_{a_1} = -n[\alpha \underline{M}_{a_1} + \alpha' \underline{M}_{a_2} + \underline{M}_{b_1} + \underline{M}_{b_2}]$$

$$\underline{H}_{a_2} = -n[\alpha'\underline{M}_{a_1} + \alpha\underline{M}_{a_2} + \underline{M}_{b_1} + \underline{M}_{b_2}]$$

$$\underline{H}_{b_1} = -n[\underline{M}_{a_1} + \underline{M}_{a_2} + \beta\underline{M}_{b_1} + \beta'\underline{M}_{b_2}]$$

$$\underline{H}_{b_2} = -n[\underline{M}_{a_1} + \underline{M}_{a_2} + \beta'\underline{M}_{b_1} + \beta\underline{M}_{b_2}]$$

where $n$, $n\alpha$, $n\alpha'$, $n\beta$ and $n\beta'$ are the Wiess constants for the interactions $A_iB_j$, $A_iA_i$, $A_iA_{j\neq i}$, $B_iB_i$ and $B_iB_{j\neq i}$ respectively and are positive for antiferromagnetic interactions.

The above equations can be rewritten in slightly different way:

$$\underline{H}_{a_1} = -n[\alpha\underline{M}_{a_1} + \alpha'\underline{M}_{a_2} + \underline{M}_{b_1} + \underline{M}_{b_2}]$$

$$= -n[\alpha\underline{M}_{a_1} - \alpha'\underline{M}_{a_1} + \alpha'\underline{M}_{a_1} + \underline{M}_B + \alpha'\underline{M}_{a_2}]$$

$$= -n[\left(\alpha - \alpha'\right)\underline{M}_{a_1} + \alpha'\underline{M}_A + \underline{M}_B] \quad \ldots\ldots\ldots\ldots\ldots\ldots (5)$$

In the same way

$$\underline{H}_{a_2} = -n[\left(\alpha - \alpha'\right)\underline{M}_{a_2} + \alpha'\underline{M}_A + \underline{M}_B] \quad \ldots\ldots\ldots\ldots (6)$$

$$\underline{H}_{b_1} = -n[\left(\beta - \beta'\right)\underline{M}_{b_1} + \underline{M}_A + \beta'\underline{M}_B]$$
$$\underline{H}_{b_2} = -n[\left(\beta - \beta'\right)\underline{M}_{b_2} + \underline{M}_A + \beta'\underline{M}_B]$$

Since the resulting magnetization of any sublattice must be parallel to the molecular field acting on that particular sublattice, it follows that $\underline{M}_{a_1}$ and $\underline{M}_{b_1}$ must be parallel to $\underline{H}_{a_1}$ and $\underline{H}_{b_1}$ respectively. Then from eqn.(5) we get that $\alpha'\underline{M}_A + \underline{M}_B$ must be parrallel or antiparallel to $\underline{M}_{a_1}$. Similarly, eqn.(6) shows that $\alpha'\underline{M}_A + \underline{M}_B$ is parallel or antiparallel to $\underline{M}_{a_2}$. So, when $\underline{M}_{a_1}$ and $\underline{M}_{a_2}$ are not parallel, we have

$$\alpha'\underline{M}_A + \underline{M}_B = 0 \qquad \ldots\ \ldots\ \ldots\ \ldots\ \ldots\ (7)$$

arguing in the same way, it can be shown that when the $\underline{M}_{B_1}$'s are not parallel

$$\underline{M}_A + \beta'\underline{M}_B = 0 \qquad \ldots\ \ldots\ \ldots\ \ldots\ \ldots\ (8)$$

If none of the magnetization vectors $\underline{M}_{a_i}$ and $\underline{M}_{b_i}$ are parallel, then $\underline{M}_A$ and $\underline{M}_B$ must satisfy the eqns. (7) and (8) simultaneously which is possible only if $\alpha'\beta' = 1$. So, in general, angle formation will not take place on both the sublattices simultaneously.

When angle formation occurs in B sublattice only we can write

$$\underline{M}_B = -\tfrac{1}{\beta'}\underline{M}_A$$

Therefore, $\underline{M} = \left(1 - \tfrac{1}{\beta'}\right)\underline{M}_A$

Since no angle exists on the A site, the two A sites are equivalent

$$\begin{aligned}\underline{H}_A &= -n\left[\alpha\underline{M}_A - \tfrac{1}{\beta'}\underline{M}_A\right] \\ &= n\left[\tfrac{1}{\beta'} - \alpha\right]\underline{M}_A\end{aligned}$$

and $\underline{H}_{b_1} = n[\beta' - \beta]\underline{M}_{b_1}$

$\underline{H}_{b_2} = n[\beta' - \beta]\underline{M}_{b_2}$

Therefore, $\underline{H}_B = n[\beta' - \beta]\underline{M}_B$

Taking the dot product of eqn. (8 ) with $\underline{M}_B$ we get

$$\left(\underline{M}_1 + \beta'\underline{M}_B\right)\cdot\underline{M}_B = 0 \qquad .. \quad .. \quad .. \quad .. \quad .. \quad (9)$$

Left hand side of this eqn is

$$\left[\left(\underline{M}_{a_1} + \underline{M}_{a_2}\right) + \beta'\left(\underline{M}_{b_1} + \underline{M}_{b_2}\right)\right]\cdot\left(\underline{M}_{b_1} + \underline{M}_{b_2}\right)$$

$$= \underline{M}_{a_1}\cdot\underline{M}_{b_1} + \underline{M}_{a_2}\cdot\underline{M}_{b_2} + \underline{M}_{a_1}\cdot\underline{M}_{b_2} + \underline{M}_{a_2}\cdot\underline{M}_{b_2} + \beta'\left(\underline{M}_{b_1} + \underline{M}_{b_2}\right)^2$$

$$= 4\underline{M}_a\underline{M}_b\cos\left(90^0 + \Psi\right) + \beta'\left(\underline{M}_{b_1}^2 + \underline{M}_{b_2}^2 + 2\underline{M}_{b_1}\cdot\underline{M}_{b_2}\cos 2\Psi\right)$$

$$= -4\underline{M}_a\underline{M}_b\sin\Psi + 2\beta'\underline{M}_b^2\left(1 - \cos 2\Psi\right)$$

where $\underline{M}_{a_1} = \underline{M}_{a_2} = \underline{M}_a$ and $\underline{M}_{b_1} = \underline{M}_{b_2} = \underline{M}_b$

Therefore eqn. (9) yields

$$2\underline{M}_a\sin\Psi = \beta'\underline{M}_b\left(1 - \cos^2\Psi + \sin^2\Psi\right)$$

or, $2\underline{M}_a\sin\Psi = \beta'\underline{M}_b\left(2\sin^2\Psi\right)$

Therefore, $\sin\Psi = \frac{1}{\beta'}\frac{\underline{M}_a}{\underline{M}_b}$

Hence such a configuration will be possible only if $\beta' \rangle \frac{\underline{M}_a}{\underline{M}_b}$

This relation at once shows that transitions between various configurations may occur in the same substance at different temperatures, without the assumption of temperature dependent interactions. For example, at T=0. a triangular configuration may exist because the above relation holds good. Now if $\underline{M}_b$ decreases faster with increasing temperature than $\underline{M}_a$, a temperature may be reached for which $\frac{1}{\beta'}<\frac{\Delta f_a}{\Delta f_b}$ and so the Neel configuration will appear before going to a paramagnetic state at $T_N$.

The Y-K spin configuration gives rise to a magnetic reflection at the normally forbidden (200) position as well as at normal spinel positions. So the existence of triangular ground states and multiple transition points can be verified by neutron diffraction experiments. Transition points can also be inferred from discontinuities in specific heat measurements. Prince [19] was the first to conclude that the neutron diffraction data on $CuCr_2O_4$ are consistent with a triangular arrangement.

# *CHAPTER 3*

## EXPERIMENTATION

## 3.1 THE TRIPLE AXIS SPECTROMETER (TAS):

The Triple axis spectrometer, as the name implies, has three axes assemblies . Fig.3.1 shows the schematic diagram of a Triple axis neutron spectrometer. A single crystal called the monochromator, oriented in an appropriate manner at an angle $\theta_M$ with respect to an incident (white) neutron beam direction, reflects neutrons of a particular wavelength ( monochromatic beam of neutrons ) along a particular direction defined by $2\theta_M$. Corresponding to this the crystal is said to have a Bragg orientation. Both $\theta_M$ and $2\theta_M$ are variable parameters. Variation of $\theta_M$ and $2\theta_M$ is achieved through drive systems consisting of a reduction gear. The movements are sensed through an optical encoder coupled to the driving shafts. The axis about which $\theta_M$ and $2\theta_M$ are varied is refrred to as the first axis. The monochromator is enclosed in a massive drum called the monochromator drum. The wall of the drum is made up of shielding materials for both neutron and gamma radiation. The monochromator drum is interfaced with the reactor beam port by an yoke assembly.

The neutron beam from the reactor passes through an entry port in the drum and is made to incident on the monochromator crystal. The monochromatic neutron beam produced as a result of Bragg reflection from the crystal passes through a Soller collimator and falls on the sample under study placed on the sample table at the second axis. These neutrons are scattered by the sample and the experiment generally involves a study of the scattered intensity as a function of the sample orientation and the scattering angle. Both these angles can be varied in a manner similar to $\theta_M$. The second axis assembly is coupled to the monochromator drum through a cantilever arrangement.

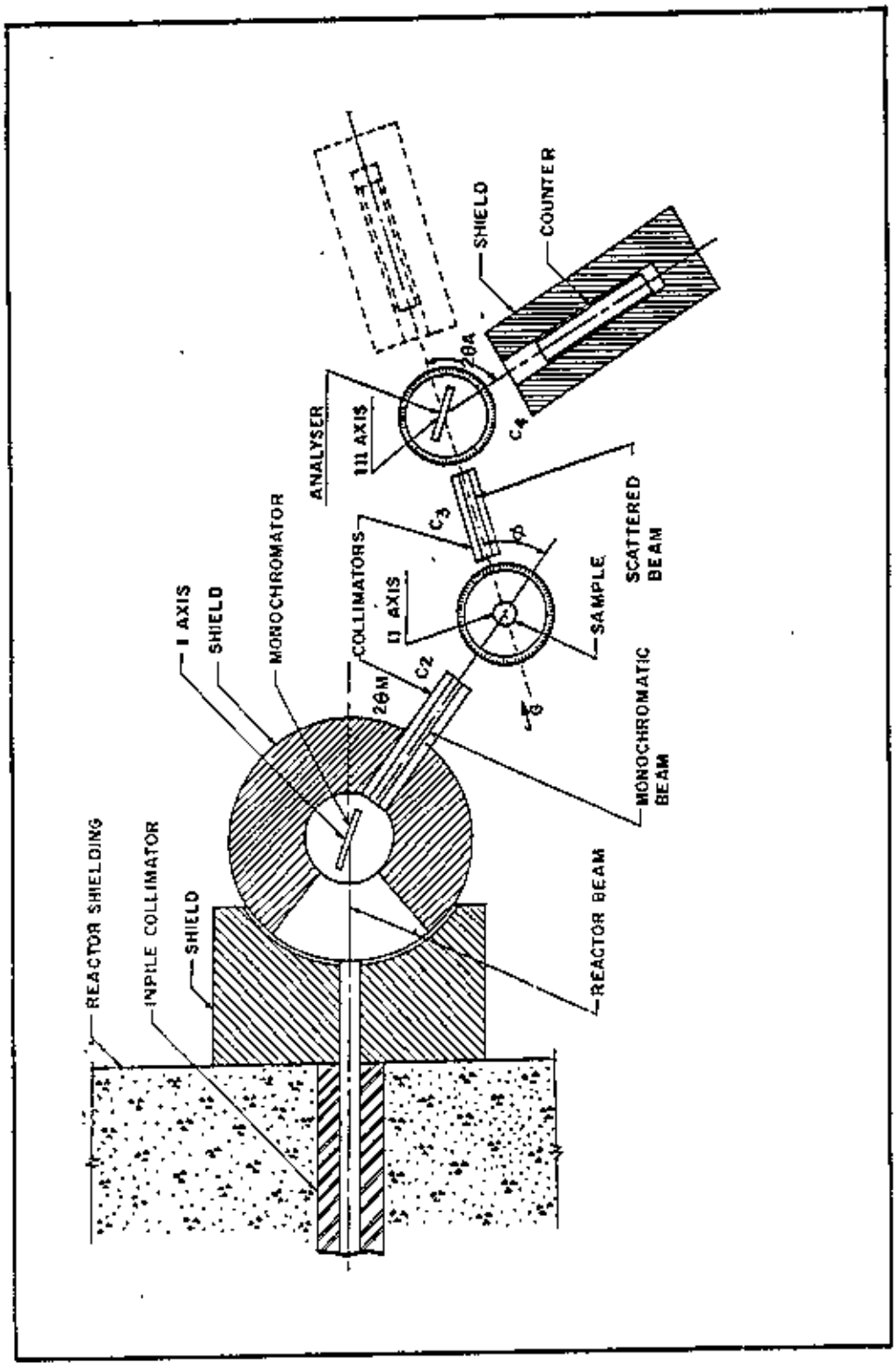


**Fig. 3.1 Schematic Diagram of the Triple Axis Spectrometer ( TAS ).**

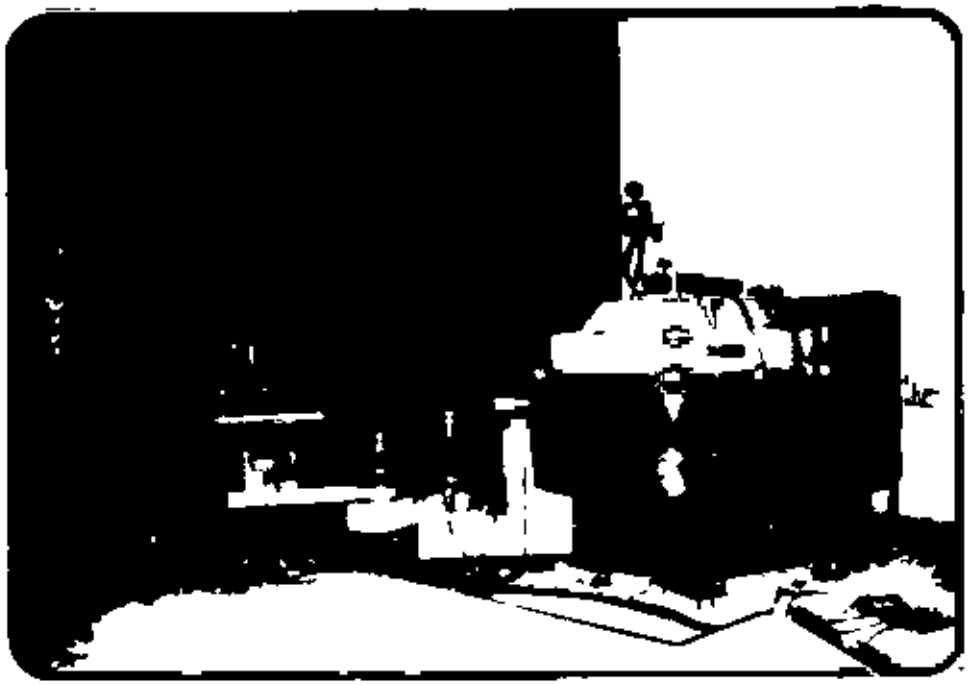

**Fig. 3.2 Photograph of the Triple Axis Spectrometer ( TAS ).**

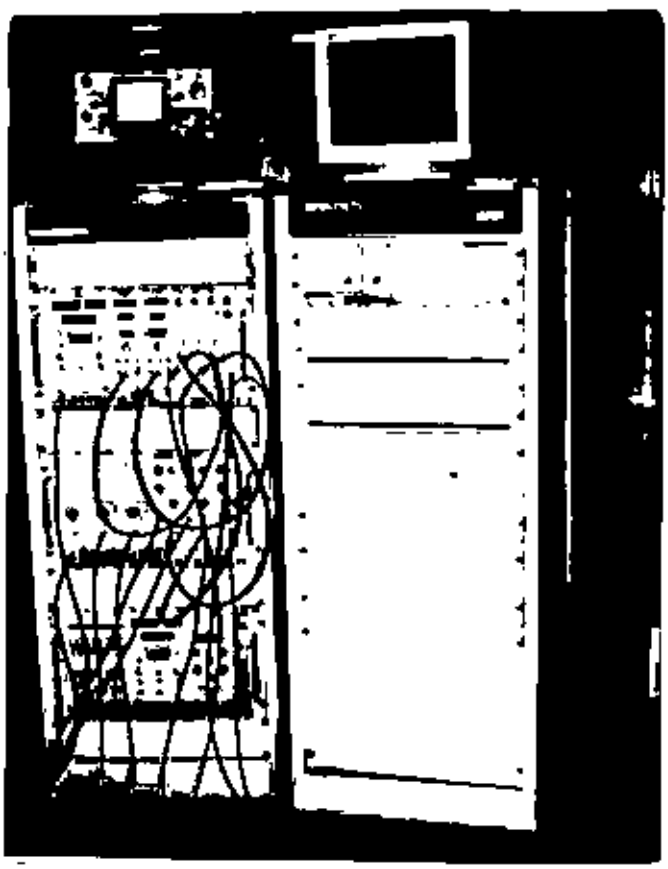

**Fig 3.3 Photograph of the Counting System ( left ) and IMDI ( right ) of the Triple Axis Spectrometer.**

The neutrons scattered in any particular direction have generally some information on the dynamics of the sample and this manifests itself through changes in the energy of the neutron. The presence of such groups of neutrons having different energy can be detected using another crystal, called the analyzer, at the third axis, which functions in a way similar to the monochromating crystal at the first axis. The angular variables associated with the angles about the third axis referred as $\theta_A$ and $2\theta_A$ enables scans over ranges of energy. Both these have motorized drives. Finally, there is a detector assembly consisting of a detector shield and a $BF_3$ detector inside the shield. The detector assembly rests on an arm which is coupled to the third axis through a cantilever. To keep track of variations in the intensity of the incident neutron beam during experiments a low efficiency neutron detector called the monitor is placed in its path. By keeping track of the number of neutrons detected by the monitor, the signal counts get normalized automatically for possible fluctuations in the monochromatic neutron beam intensity.

The spectrometer is fully automatic and computerized. The motions of all the motor drives, recording of data and counting time of the detector is controlled through electronic control system and a 80286 PC/AT computer. The counting system is connected to a control system called the intelligent motor drive unit (IMDI) which has a inbuilt mini computer. There is a status monitor attached to the IMDI which shows the present status of all the motor drives. The programs for controlling the spectrometer and acquiring data from it can be designed as per requirement of a particular experiment by using the programming languages. The typical programs consist of commands to move the motors to various positions according to some predefined algorithm and acquiring pertinent data at each point. The IMDI receives commands from the host computer and accordingly executes them. It has a permanent soft ware called firm ware and there are several soft

wares in the host computer. The experiments are set by loading the controlling program in the host computer. Once the program is loaded the entire experiment is carried on automatically and the obtained data is also stored in the host computer. It is possible to record data at angular steps as small as 0.01 deg. Fig.3.2 shows a photograph of the actual spectrometer and Fig 3.3 is the photograph of the IMDI and the counting system.

## 3.2 EXPERIMENTAL PROCEDURES:

The experiment consists of two parts namely the study of the performance data of the spectrometer and determination of the atomic and magnetic structure of a Ni-Zn ferrite. The first part of the experiment was accomplished in three successive steps. Firstly, the Cu ( 002 ) monochromator of the spectrometer was aligned to set it at the correct zero-Bragg-angle position to reflect a monochromatic neutron beam. For this the monochromator axis ( first axis ) was rotated by a d.c. motor in steps of 0.2 deg. and at each step the detector counts were recorded for a fixed monitor count. This movement of motor and recording of data at each angular position were controlled through a soft ware called PDIFF by giving necessary input. A rocking curve was plotted to find out the correct zero-Bragg-angle position ( Fig.3.4 ).

Secondly, the alignment of the detector was checked to set it at the correct zero-line of the spectrometer. This zero-line corresponds to the direction of the incident neutron beam and is the reference line for all positional measurements. This was accomplished through the movement of

another d.c. motor following the same procedure as above except that this time the detector was rotated keeping the monochromator fixed at the zero-Bragg-angle position. The correct zero-position of the detector was found out from the counts vs. detector angle graph (Fig.3.5).

Finally, to test the performance data produced by the spectrometer a diffraction run were taken with a standard aluminium sample The sample was in the powdered form and was supplied by the manufacturer of the spectrometer ( BARC, India ) for testing the performance of the spectrometer. It was put in a quartz container in a tightly packed condition and was placed in the neutron beam on the sample table of the spectrometer. Using the same computer program PDIFF scanning of the diffraction lines ranging from 25 - 82 deg. in steps of 0.2 deg. for a fixed monitor counts was done. Since there may be fluctuation in the reactor flux during the experiment, the preset monitor counting method was adopted where the detector records the counts for a preset value of the monitor counts. A similar scanning was done for the empty quartz container and the obtained data were subtracted from those obtained with the sample in the container in order to eliminate the contribution of the container to the diffraction data. The experiment was done at 3 MW power level of the TRIGA MARK II reactor at the Atomic energy Research Establishment, Savar, Dhaka. The neutron wavelength used in the experiment was 1.24Å corresponding to ( 002 ) reflection of the copper monochromator setting at a take off angle of 20deg.

In the second part of the experiment a nickel-zinc mixed ferrite having composition $Zn_{0.55}Ni_{0.35}Fe_2O_4$ was studied. The sample was prepared in the laboratory of the Magnetic Materials Division of Atomic Energy Center, Dhaka. The usual ceramic sintering process was employed to prepare it. The oxides $Fe_2O_3$, ZnO and NiO were mixed up intimately by ball milling in the ratio of

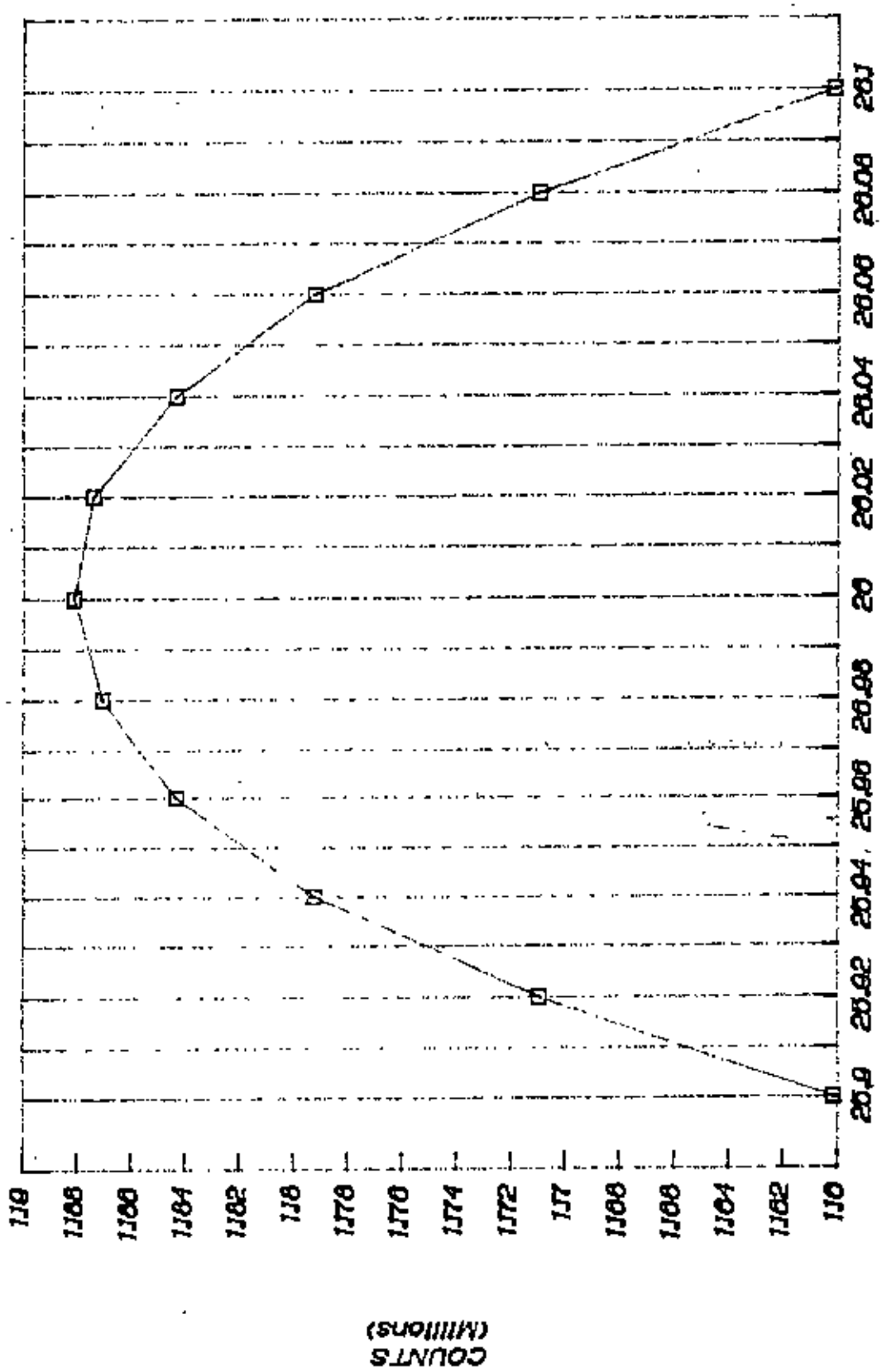


Fig. 3.4 Alignment of Cu ( 002 ) Monochromator of TAS.

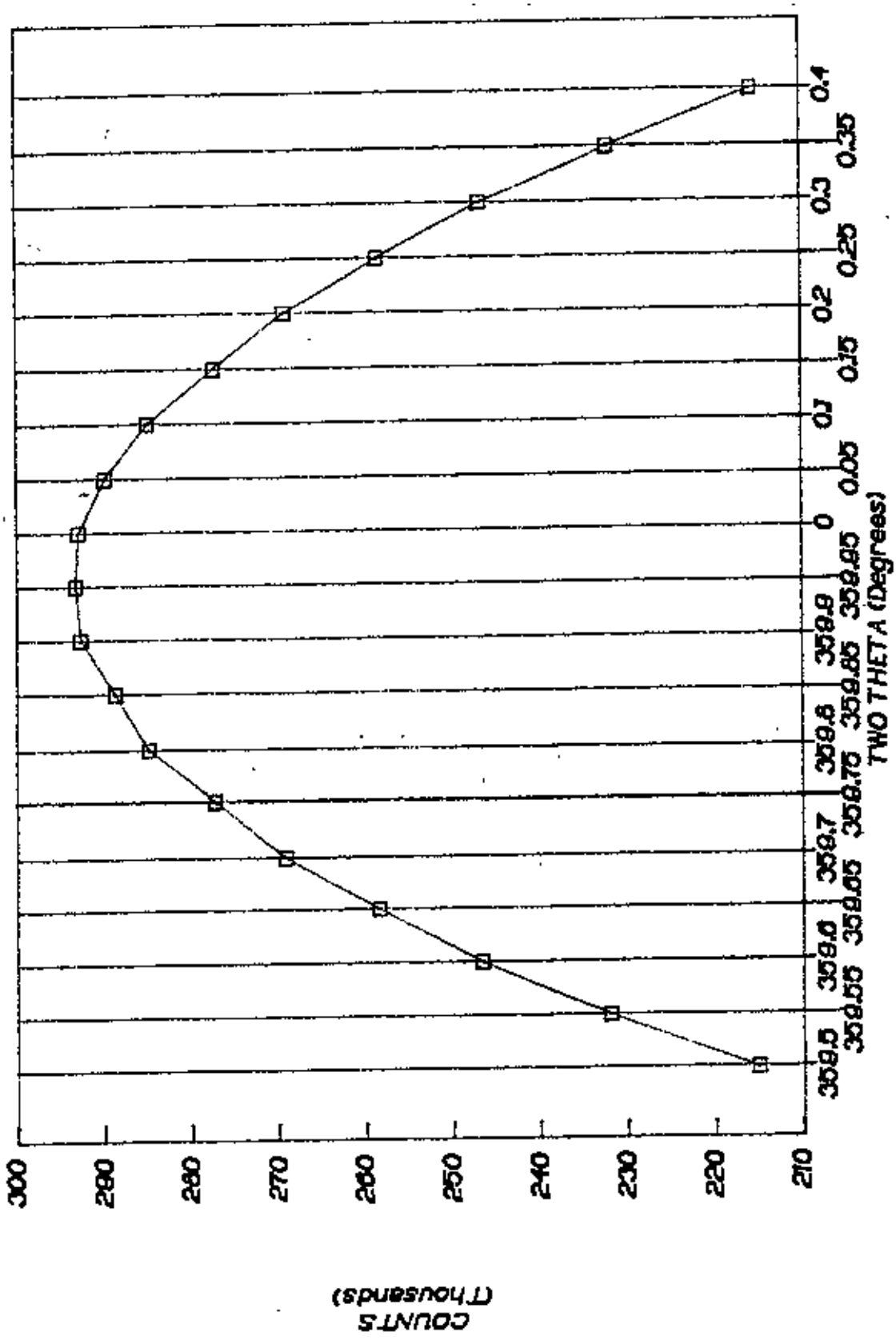


Fig. 3.5 Alignment of the Detector ( $BF^3$ ) of TAS.

1.85, 0.85 and 0.15 molecular percent to give the correct stoichiometric proportion and then presintered at a temperature of 1050$^0$C for three hours. The resulting powder was compressed into cylindrical rods of 8.5 mm dia. and 60 mm in length. The rods were sintered in air at 1150$^0$C for three hours and then slowly cooled in a furnace. A 33 mm long piece of it was put on the sample table of the spectrometer and a diffraction run at room temperature was taken in the same process as used in the case of aluminium. This experiment was also conducted at the 3 MW power level of the reactor and the wave length of the monochromatic neutron beam reflected from the Cu ( 002 ) monochromator was also kept 1.24Å. 2θ scanning , ranging from 10- 74.4 deg. with step width of 0.2 deg. of the diffracted beams from the sample, was carried out twice At each step of scanning the detector couts were recorded for a preset monitor counts of 250000. Out of the two sets of data, the best one was used for the analysis. The X-ray diffraction of the same sample was done from the Bangladesh University of Engineering and Technology, Dhaka.

# *CHAPTER 4*

## COMPUTATION AND DATA ANALYSIS

In a polycrystalline sample, it is inevitable that certain information is lost due to the random orientation of the crystallites. The data relate purely to interplanar separations and all the directional information is lost. A more serious loss of information is due to the overlap of independent diffraction peaks in the powder diagram. If the sample under study possesses a simple structure with a small unit cell, it is practicable to separate out from the pattern the discrete peaks and hence the structure factors for individual reflections. These observed normalized values can be fitted to a structural model by the method of least-squares refinement. With overlapping peaks, however the mode of treatment of data changes significantly. The conventional method using the total integrated intensities of the separate groups of overlapping peaks in the least-squares refinement of structures, leads to the loss of all information contained in the often detailed profile of the composite peaks. In the Rietveld method[39] the profile intensities has been used instead of the integrated quantities in the refinement procedure. This method allows the extraction of the maximum amount of information contained in the powder diagram[21].

## 4.1 The Rietveld Method:

For all crystal systems of high symmetry, contribution from several different crystal reflections will arrive at any given position $2\theta$ in the diffraction pattern. Each reflection will have an angular width which is dependent on the neutron spectral distribution, monochromator mosaic distribution, the collimating system i. e. the transmission function of the Soller collimator and the

sample crystallinity. In practice it is found that the convolution of all these contributions is almost exactly Gaussian, except at very low angles; this fact is very elegantly exploited in the profile refinement method.

In a powder diffraction pattern with a small number of overlapping peaks, a group of them can be considered as a single observation and conventional refinement carried out. Though it is not practicable to separate out the discrete peaks from the pattern and hence the structure factors for individual reflections, the Rietveld method considers each point on the profile as a single observation which may contain contributions from a number of different Bragg reflections. The shape of each Bragg reflection is assumed to be Gaussian. Thus at any angular position, the resultant of the overlapping contributions can be calculated in terms of a series of parameters which can be obtained by the method of least squares.

Assuming a Gaussian peak shape for each Bragg reflection, the observational equations for profile refinement is written as

$$y_i = kt\, S_k^2 j_k L_k \frac{2\sqrt{\ln 2}}{H_k\sqrt{\pi}} \exp\{-4\ln 2\left[\frac{(2\theta_i - 2\theta_k)}{H_k}\right]^2\}$$

where $y_i$ = the profile intensity,

k = scale factor

t = step width of the detector

$S_k^2 = F_k^2 + J_k^2$ , the sum of the nuclear and magnetic contributions respectively.

$j_k$ = multiplicity of the reflection

$L_k$ = lorentz factor of the reflection

$2\theta_k$ = calculated position of the Bragg peak corrected for zero point shift of the detector.

$H_k$ = the full width at half maximum.

The angular width $H_k$ of the Gaussian peaks varies with $2\theta$ and is given by [22] :

$$H_k^2 = U\tan^2\theta_k + V\tan\theta_k + W$$

where U,V,W are half width parameters.

If we put $I_k = S_k^2 j_k L_k$ and

$$G_{ik} = \frac{2\sqrt{\ln 2}}{H_k\sqrt{\pi}} \exp\{-4\ln 2[(2\theta_i - 2\theta_k)/H_k]^2\}$$

the profile intensity can be written as

$$y_i = kI_k G_{ik}$$

$G_{ik}$ represents the normalized Gaussian centered at $2\theta_k$ with a variance of $2\sqrt{\ln 2/H_k}$ and is a function of the profile parameters ( $p_p$ ) alone. The structural parameters ($p_c$ ) affect only the $I_k$ and these are of direct interest in any diffraction experiment. Thus $y_i$ can be written as

$$y_i = M_k ( k, p_c ) G_{ik} (i, k, p_p )$$

Thus for a single resolved peak at $2\theta_k$, each intensity measurement on the profile gives an estimate of the same Bragg intensity and gives different information concerning the profile parameters alone. No additional structural information can be gained by increasing the number of points on the profile. This only increases the effective precision which can be gained in the determination of the Bragg intensity.

## 4.2 Profile Calculations:

As the tails of a Gaussian peak decrease rather rapidly, the peak is assumed to extend 1.5 times the half width to both of its central position. In case of overlap, more than one Bragg peak contributes to the profile intensity $y_i$

$$\text{i. e. } y_i = \Sigma_k k I_k G_{ik},$$

where the summation is over all the reflections which can theoretically contribute to $y_i$ on the basis of their position $2\theta_k$ and their half widths $H_k$. For larger scattering angles and for crystals with a

low symmetry this summation can be over more than ten terms. On the other hand, those regions of the diffraction pattern, where no peaks can possibly contribute, are left out of the calculations.

If a single Bragg peak is measured by n profile points, we will have n equations for $y_i$ with i running from $i_0$ to $i_0$ – n-1.

$$\begin{aligned} y_{i0} &= kI_k G_{i0,k} \\ &\vdots \\ y_{i0+n-1} &= kI_k G_{i0+n-1,k} \end{aligned} \qquad \text{(A)}$$

Summing these equations we get

$$\sum_{j=0}^{n-1} y_{i0-j} = kI_k \sum_{j=0}^{n-1} G_{i0+j,k}$$

for large n, $\sum_{j=0}^{n-1} G_{i0+j,k} \rightarrow 1$,

therefore, $\sum_{j=0}^{n-1} y_{i0+j} = kI_k$ (B)

Equations ( B ) are the observational equations for the profile refinement method, whereas ( A ) is for the conventional integrated intensity refinement. The structural information is the same in both cases, only information concerning the profile parameters has been lost in the summation

In the profile analysis the deviations of the peak profile from an expected Gaussian shape due to peak asymmetry and preferred orientation have to be accounted for by using semi-empirical corrections. Peak asymmetry arises mainly due to the finite slit heights together with finite sample heights; the peak maximum shifts to lower angles but does not affect the integrated peak area and introduction of the asymmetry parameter gives a good approximation to the asymmetric peak profile. Introduction of the preferred orientation parameter gives a measure of the half width of the assumed Gaussian distribution of the normals of the crystallites about the preferred orientation direction [23].

## 4.3 Least-Squares Refinement:

Profile refinement would mean the minimizing of

$$\Delta = \Sigma_i w_i \left( y_i - k \Sigma_k I_k G_{ik} \right)^2$$

where $w_i$ = weight of the corrected intensity $y_i$

$\Sigma_k$ = sum over different Bragg peaks and
$\Sigma_i$ = sum over a single Bragg peak.

The weights used are

$$w_i = 1/[\sigma^2(y_i) + \sigma^2(B_i)]$$

$\sigma^2(B_i)$ is negligible as it is a graphically determined quantity, and hence $w_i = 1/[\sigma^2(y_i)]$

As the problem is not linear in the parameters, approximate values for all parameters are required for the first refinement cycle. These are refined in subsequent refinement cycles until a certain convergence criterion has been reached. The parameters which can be refined include the half -width parameters, counter zero point, cell parameters, possible asymmetry of the diffraction peaks and preferred orientation parameter as well as the structure parameters. The quantitative agreement between observed and calculated intensities can be judged by defining the following R-factors.

$$R_{profile} = 100x \sum_i |y_i(obs) - \tfrac{1}{k} y_i(calc)| / \sum_i y_i(obs),$$

Weighted profile R-factor =

$$R_{wp} = 100 \times \left[ \sum w_i \left( y_i(obs) - \tfrac{1}{k} y_i(calc) \right)^2 / w_0 y_i^2(obs) \right]^{\frac{1}{2}},$$

$$R_{total} = 100x \sum_i |S_i^2(obs) - \tfrac{1}{k} S_i^2(calc)| / \sum_i S_i^2(obs),$$

$$R_{nuclear} = 100x \sum_i |F_i^2(obs) - \tfrac{1}{k} F_i^2(calc)| / \sum_i F_i^2(obs),$$

$$R_{magnetic} = 100x \sum_i |J_i^2(obs) - \tfrac{1}{k} J_i^2(calc)| / \sum_i J_i^2(obs).$$

Where, $F_i^2, J_i^2 and S_i^2$ are the nuclear, magnetic and total structure factors respectively. There is another R-factor called $R_{expected}$ defined as

$$R_{expected} = 100 \times \left[ (N - P + C) / \sum w_i y^2(obs) \right]^{\frac{1}{2}}$$

where, (N- P + C) is the number of degrees of freedom with

N = the number of points in the pattern,

P = the number of refined parameters and

C = the total number of constraints.

Using the Rietveld refinement method, one can extract maximum available information from a powder diagram as against any peak separation method. The technique has been proved extremely valuable for determination of small parameter changes which take place in ferroelectric and antiferroelectric transitions. However, the more the overlap between Bragg peaks, more is the uncertainty associated with the individual integrated intensities and the precision and accuracy of the parameters will depend directly on the goodness-of-fit of the model to the data.

## 4.4 Analysis of the Diffraction Data of the Samples under Present Study:

The computation and analysis of the diffraction data from the samples aluminium and Ni-Zn ferrite under study were carried out using a 486 P. C. in the neutron scattering laboratory of the Institute of Nuclear science and Technology, Savar, Dhaka. The above discussed Rietveld method was employed to analyze those data. Two different versions of the Rietveld refinement program ---- RIET and FULLPROF were used in the present analysis. Basically both the versions

are same except that the second one takes into account the magnetic contribution in addition to the nuclear contribution. The first one was used to analyze the data of aluminium and the second one was employed to analyze the data of Ni-Zn ferrite. Both the programs were run in the above mentioned computer.

Crystal structure analysis consists in finding a structure whose diffraction spectra match the observed set. Once a model of the crystal structure is available which gives fair agreement between the observed and calculated intensities, further refinement of the model is usually carried out using a crystallographic least square procedure. The essential function of a least squares program is the adjustment of the parameters of the model, i.e the atomic positions, temperature factors and site occupation parameters in such a way as to minimize the sum of the squares of the weighted differences between observed and calculated values of intensities from the fitted curve. According to the space group and other given inputs the program generates a calculated pattern and then tries to fit with the observed pattern as discussed above. The necessary input parameters were varied through out the refinement process by allocating a code number to each of them to achieve best possible fit. The parameters which were varied through out the refinement process are listed in the table 4.1.

# TABLE 4.1

## Parameters Varied in the Refinement Process

| $X_i$ | $Y_i$ | $Z_i$ | $B_i$ | $N_i$ | $K_{x_i}$ | $K_{y_i}$ | $K_{z_i}$ | $\beta_{11_i}$ | $\beta_{22_i}$ | $\beta_{33_i}$ | $\beta_{12_i}$ | $\beta_{13_i}$ | $\beta_{23_i}$ |
|---|---|---|---|---|---|---|---|---|---|---|---|---|---|
| ⋮ | | | | | | | | | | | | | |
| ⋮ | | i = 1,N | | | | | | | | | | | |
| ⋮ | | | | | | | | | | | | | |
| ⋮ | | | | | | | | | | | | | |
| G | P | - | Q | 1/C | | | | | | | | | |
| U | V | W | Z | a | b | c | α | β | γ | | | | |

In table 4.1 $x_i$, $y_i$, $z_i$ is the fractional position coordinate, $B_i$ is the isotopic atomic temperature factor, $N_i$ is the occupation number. $K_i$'s are the components of the atomic magnetic moments and $\beta_i$'s are the anisotropic temperature factors for the ith atom. G is the preferred orientation parameter, P is the asymmetry parameter, Q is the over all temperature factor and 1/C is the scale factor. U, V, W are the half width parameters, Z is the zero point position of the counter and a, b, c, α, β, γ are the cell constants. In the refinement procedure the background counts were matched through fitting a polynomial by the program. The space group for aluminium sample was Fm3m and that for ferrite sample was Fd3m. According to the given structural and profile parameters and with the symmetry of this space group the program generates a calculated diffraction pattern and then verifies the degree of matching with the observed pattern. This degree of matching is justified by the different R-factors.

# *CHAPTER 5*

## RESULTS AND DISCUSSIONS

## 5.1 PERFORMANCE DATA OF THE TRIPLE AXIS SPECTROMETER

The performance of the Triple axis spectrometer was tested by determining the zero-Bragg-angle position of the monochromator and the zero-position of the detector (Spectrometer Zero-line) and then performing neutron diffraction study of a standard aluminium sample with this set-up and checking the reproducibility of diffraction pattern by the spectrometer.

### i) Determination of Zero-Bragg-angle Position and Spectrometer Zero-line:

The monochromator used in the spectrometer was Cu ( 002 ) single crystal which has a d-spacing of $1.81\mathring{A}$. The zero-Bragg-angle position of the monochromator is the position at which ( 002 ) plane of the crystal is correctly oriented with respect to a particular wavelength of the incident neutron beam from the reactor for Bragg reflection. Correct determination of this position is an essential prerequisite for any neutron diffraction experiment. At this position the intensity of the reflected beam for a particular neutron-wavelength is highest. In the present measurement, the correct zero-Bragg-angle position ($\theta$) was found out from the rocking curve for the crystal obtained by plotting the measured intensity vs. crystal orientation keeping the detector at a fixed position ($2\theta$). The zero-Bragg-angle position ($\theta$) determined from this rocking curve of the monochromator ( Fig.3.4 ) was $26^0$. But the zero position of the scale of the first axis which holds the monochromator of the spectrometer is $6^0$. Therefore the corrected value of zero -Bragg-angle is $20^0$. Thus the wavelength of the monochromatic neutron beam produced as a result of Bragg reflection from the monochromator crystal was $1.24\mathring{A}$. The neutrons of this wavelength were used for the diffraction experiments performed on the samples under study.

The approximate zero-line of the spectrometer was found to be $359.95^0$ from the graph of Fig.3.5. The zero-line plays a very important role in the accuracy of experiments performed by the spectrometer, since the angular positions of the diffraction lines are measured with respect to this position. Actually the incident neutron beam is directed along this line. Bragg angle ( $\theta$ ), which is the angle between the incident beam and the net reflecting plane of the crystal, can not be measured experimentally. What is measured experimentally is the angle between the incident beam and the diffracted beam which is twice the Bragg angle and is known as scattering angle ( $2\theta$ ). The approximate zero position was found to be $359.95^0$ from Fig.3.5 which is a plot of intensity as a function of scattering angle obtained by scanning the detector around the second axis for a fixed monochromator position. The correct zero-position of the detector determined from the Rietveld refinement of the diffraction data of standard aluminum sample was $359.91°$.

## ii) Neutron Diffraction Study of Standard Aluminium Powder Sample:

Aluminium has a f.c.c structure and it belongs to the space group Fm3m. It has a cubic close packing array with 4 atoms per unit cell located at the positions

**4a: (0 0 0 ), F. C.**

The neutron diffraction pattern of aluminium contains sharply defined and well separated Bragg peaks. Thus aluminium is considered as an ideal standard sample to study the performance of a diffractometer. In the present study a diffraction run from $25^0$ to $82^0$ of powdered aluminium sample was taken. The diffraction data obtained in this experiment were analyzed by the Program RIET using the Rietveld refinement method. The observed and calculated intensity for each reflection has been listed in Table 5.1.

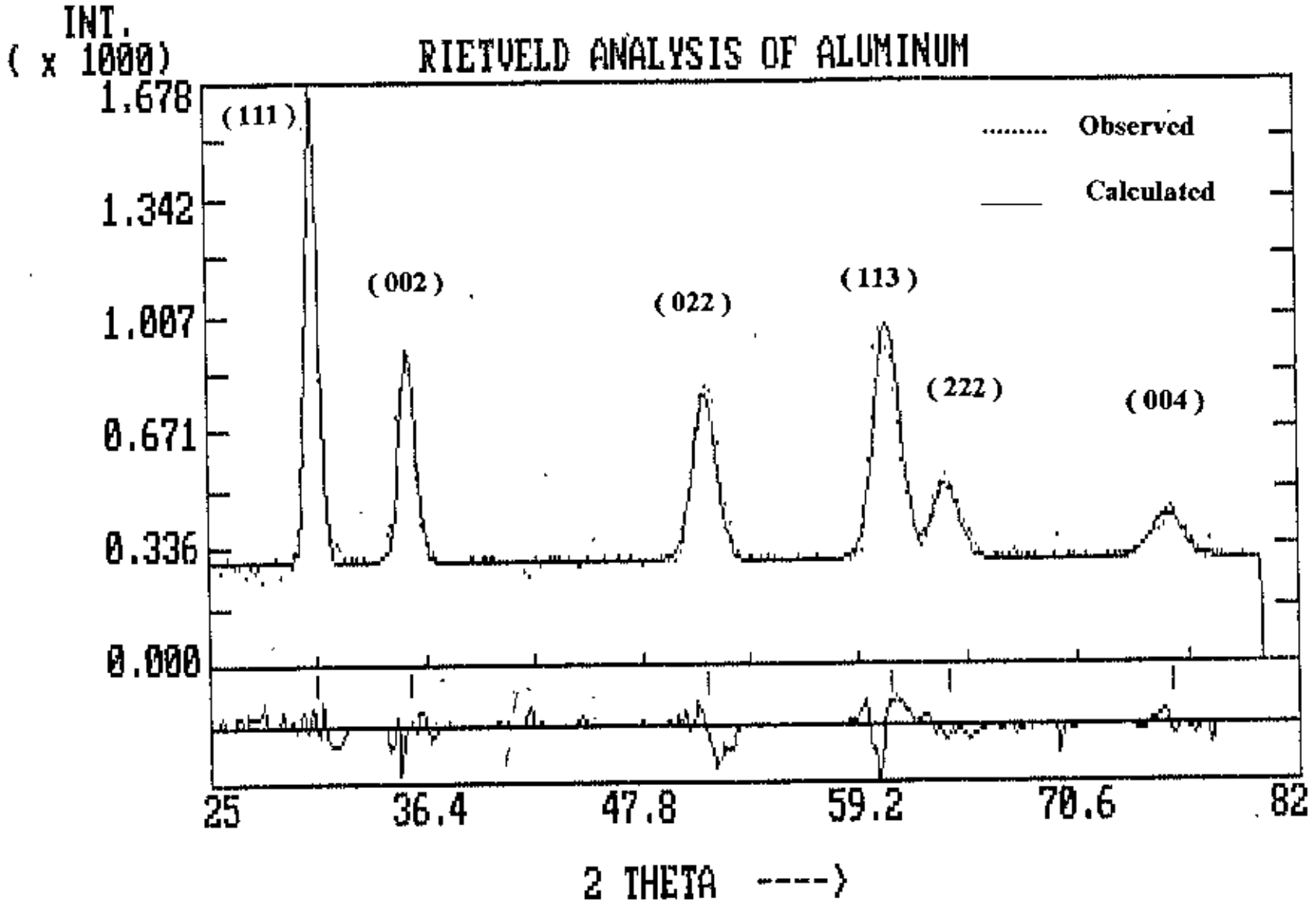


Fig. 5.1 Fitted Neutron Diffraction Pattern of Aluminium.

# TABLE 5.1

## Comparison of the refined values of observed and calculated intensities of powdered $Al_2$ sample

| (h k l) | Multiplicity | Scattering Angle (Deg.) | Calculated Intensity | Observed Intensity |
|---|---|---|---|---|
| (1 1 1) | 8 | 30.687 | 137310 | 138228 |
| (0 0 2) | 6 | 35.582 | 79629 | 81700 |
| (0 2 2) | 12 | 51.202 | 90635 | 92873 |
| (1 1 3) | 24 | 60.887 | 145810 | 144543 |
| (2 2 2) | 8 | 63.905 | 46119 | 45759 |
| (0 0 4) | 6 | 75.336 | 29954 | 30178 |

$R_{wp}$ = 1.17 $R_{profile}$ = 3.90

$R_{expected}$ = 5.07

Fig. 5.1 shows the fitted pattern of Aluminium. From the Table 5.1 and also from the goodness of fit it is evident that agreement between the observed and the calculated pattern generated by the program was quite satisfactory. The different R-factors listed under the Table 5.1 obtained from the refinement indicate a quantitative measure of this agreement. All the Bragg peaks produced were prominent and well distinguishable. The position of each of the Bragg peaks in the observed pattern matched very well with those in the calculated pattern which indicated a very good reproducibility of diffraction data by the spectrometer. The cell dimension obtained through this refinement was $4.047\mathring{A}$ which is in good approximation with the value $4.049\mathring{A}$ available in literature[24].

Thus from the very good matching of the diffraction pattern with that of the calculated one obtained from the neutron diffraction study of the standard aluminium sample and from the good agreement of the measured crystal structure parameter with that in the standard literature, a good performance of the spectrometer is well established.

## 5.2 CRYSTAL AND MAGNETIC STRUCTURE OF Ni-Zn FERRITE

### i) Crystal Structure Parameters:

In the analysis of the observed diffraction data by the FULLPROF program the nuclear and magnetic contribution were refined separately in two different phases. The values of the observed and calculated intensities for all the reflections as found out from the refinement of the experimental data in the nuclear phase has been listed in the Table 5.2. It can be seen that there is a good agreement between the observed and calculated intensities. The different R-factors listed under the table also indicate a qualitative measure of this agreement. All the crystal structure parameters obtained as a result of this refinement process are discussed below.

In the case of spinels mainly three crystallographic parameters are to be determined. These are:

i) Cation distribution on the A and B sites,

ii) Unit cell dimension $a_0$ ,

iii) Oxygen position parameter, u.

# TABLE 5.2

**Comparison of the refined values of the observed and calculated intensities for $Zn_{0.85}Ni_{0.15}Fe_2O_4$ in the nuclear phase.**

| (h k l) | Multiplicity | Scattering angle (Deg.) | Calculated Intensity | Observed Intensity |
|---|---|---|---|---|
| (1 1 1) | 8 | 14.625 | 828 | 1058 |
| (2 2 0) | 12 | 23.992 | 355 | 365 |
| (3 1 1) | 24 | 28.212 | 1958 | 2126 |
| (2 2 2) | 8 | 29.494 | 38 | 29 |
| (4 0 0) | 6 | 34.187 | 2404 | 2238 |
| (3 3 1) | 24 | 37.363 | 8 | 8 |
| (4 2 2) | 24 | 42.200 | 174 | 234 |
| (5 1 1) | 24 | 44.894 | 1798 | 1826 |
| (3 3 3) | 8 | 44.894 | 69 | 70 |
| (4 4 0) | 12 | 49.125 | 4268 | 4185 |
| (5 3 1) | 48 | 51.537 | 408 | 326 |
| (4 4 2) | 24 | 52.323 | 12 | 11 |
| (6 2 0) | 24 | 55.388 | 73 | 116 |
| (5 3 3) | 24 | 57.614 | 538 | 647 |
| (6 2 2) | 24 | 58.344 | 6 | 6 |
| (4 4 4) | 8 | 61.209 | 975 | 973 |
| (7 1 1) | 24 | 63.306 | 2 | 2 |
| (5 5 1) | 24 | 63.306 | 467 | 326 |
| (6 4 2) | 48 | 66.720 | 264 | 326 |
| (7 3 1) | 48 | 68.726 | 220 | 256 |
| (5 5 3) | 24 | 68.726 | 785 | 915 |
| (8 0 0) | 6 | 72.011 | 1007 | 1011 |

$R_{nuclear} = 4.56$ $R_{expected} = 7.07$

Neutron diffraction results have established inverse spinel and normal spinel structures for $NiFe_2O_4$ and $ZnFe_2O_4$[8] respectively. $Ni^{2+}$ ions in the former occupy the octahedral (B) sites and $Zn^{2+}$ ions in the latter occupy the tetrahedral ( A ) sites. A mixed system $Zn_xNi_{1-x}Fe_2O_4$ is neither inverse spinel nor normal spinel but has a structure in between the two. In this structure, $Zn^{2+}$ and $Ni^{2+}$ ions should still occupy A and B sites respectively. Neutron diffraction study of such a mixed ferrite $Zn_{0.5}Ni_{0.5}Fe_2O_4$[25] supports this. The occupation of various sites by the cations in the sample $Zn_{0.85}Ni_{0.15}Fe_2O_4$ under present study was carefully determined. This was accomplished during the data refinement process through interchanging octahedral and tetrahedral position coordinates alternately among the $Zn^{2+}$ and $Ni^{2+}$ ions. It was found that the $Zn^{2+}$ and $Ni^{2+}$ ions invariably occupy the tetrahedral and octahedral sites respectively which are in agreement with the previously reported distribution scheme. $Fe^{3+}$ ions were found to occupy both the A and B sites simultaneously as expected in the case of a mixed structure. The cation distribution found in this mixed ferrite system can thus be written as:

$$( Zn_{0.85}Fe_{0.15} )[Ni_{0.15}Fe_{1.85}]O_4$$

where ( ) and [ ] denotes the A and B sites respectively. The Table 5.3 shows the crystallographic sites occupied by various ions, their chemical occupation number and the obtained cation distribution for the sample under study.

# TABLE 5.3

## Ionic Distribution in $Zn_{0.85}Ni_{0.15}Fe_2O_4$

| Ions | Crystallographic Site | Chemical Occupation number | Cation Distribution |
|---|---|---|---|
| $Zn^{2+}$ | 8a | 0.85 | |
| $Fe^{3+}$ | 8a | 0.15 | |
| $Fe^{3+}$ | 16d | 1.85 | $(Zn_{0.85}Fe_{0.15})[Ni_{0.15}Fe_{1.85}]$ |
| $Ni^{2+}$ | 16d | 0.15 | |
| $O^{4-}$ | 32e | 4 | |

The oxygen coordinate of a ferrite system mentioned in section 2.4 of chapter 2 possesses a variable parameter u which needs to be measured precisely in order to get a correct picture of the structure. The tetrahedral sites which are smaller than the octahedral sites are too small to contain a metal ion. As discussed diagrammatically ( Fig.2.3 ) in chapter 2 a consequence of this is that there is an expansion in the tetrahedral site. On the other hand there will be an equal amount of shrinkage in the octahedral site. As a result of this the oxygen positions in a spinel lattice are variable. The parameter u in the oxygen coordinate is a measure of this variations. As a result of this expansion and contraction of the two lattice sites, the unit cell dimension $a_0$ in the ferrite system also becomes a variable parameter. Both of these parameters are thus strongly dependent on the dimension of the cations at the different sites.

The observed cation distribution for the sample under present study shows that most of the A sites have been occupied by $Zn^{2+}$ ions which have larger dimension ( $0.83\mathring{A}$ ) in comparison with those of the other two cations $Ni^{2+}$ ions (dim. = $0.78\mathring{A}$ ) and $Fe^{3+}$ ions ( dim. = $0.67\mathring{A}$ ). Again, Guillaud[26] showed that the higher is the concentration of zinc in a Ni-Zn mixed ferrite, the higher is the cell dimension. As the present sample contains a very high concentration of zinc, the cell dimension and also the oxygen parameter u will be larger in this case than any other sample having less concentration of zinc. These two quantities were measured very precisely from the refinement procedure. The cell dimension was measured both by X-ray diffraction and neutron diffraction method. The measured values have been presented in the Table 5.4 below along with the values obtained by N. S. Satya Murthy et al.[9] from X-ray and neutron diffraction studies of the sample $Zn_{0.75}Ni_{0.25}Fe_2O_4$.

# TABLE 5.4

## Comparison of the cell dimension $a_0$ and u parameter of $Zn_{0.85}Ni_{0.15}Fe_2O_4$ and $Zn_{0.75}Ni_{0.25}Fe_2O_4$

| Sample | Reference | $a_0$ ( Angstrom ) | u |
|---|---|---|---|
| $Zn_{0.75}Ni_{0.25}Fe_2O_4$ | ( 9 ) | X-ray Diffraction: 8.400<br>Neutron Diffraction: --- | Neutron Diffraction: 0.2598 |
| $Zn_{0.85}Ni_{0.15}Fe_2O_4$ | Sample under present study | X-ray Diffraction: 8.44<br>Neutron Diffraction: 8.412 | Neutron Diffraction: 0.2614 |

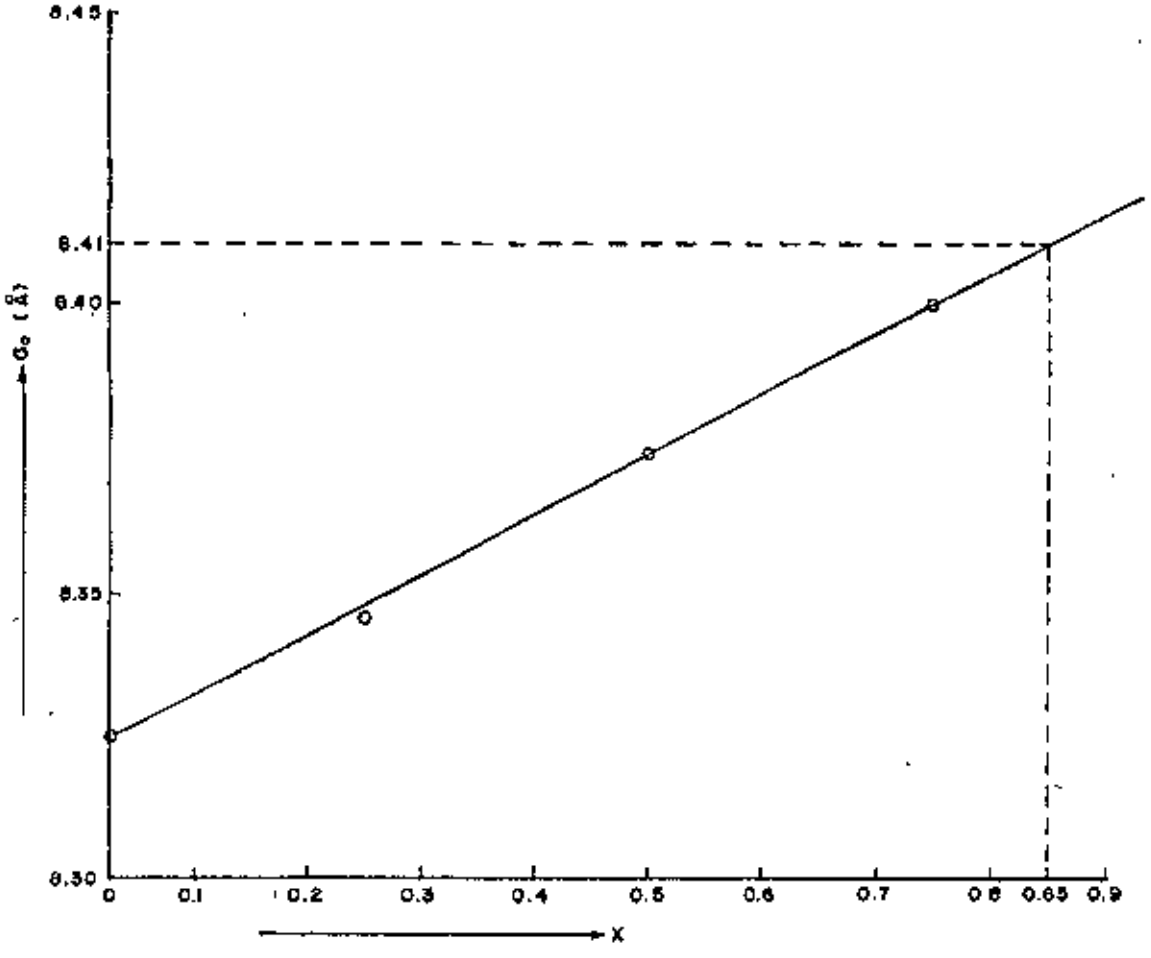


**Fig. 5.2 Cell Dimension as a function of x as measured by N. S. Satya Murthy et al.**

N. S. Satya Murthy et al. studied the mixed ferrite $Zn_xNi_{1-x}Fe_2O_4$ with four different concentrations of zinc ( x values ) of which the composition $Zn_{0.75}Ni_{0.25}Fe_2O_4$ is close to the sample under present study and different parameters of this sample as determined by them has been compared with those of the sample under present study in Table 5.4. The content of zinc is 10 molecular percent higher in our sample than that of this sample. The Table 5.4 shows that both the cell dimension and the oxygen parameter values are little larger in our case which is in accord with the above reasonings. Fig.5.2 is a plot of cell dimension as a function of x as measured by Satya Murthy et al. From the extrapolation of this curve the cell dimension for our sample ( x = 0.85 ) is found to be 8.41$\mathring{A}$. Our measured value 8.412$\mathring{A}$ is in good agreement with this in the first approximation. Fig.5.3 shows the X-ray diffraction pattern of the same sample. By comparing this pattern with the neutron diffraction pattern ( Fig.5.4 ) of the sample it can be seen that many peaks which are present in the neutron pattern, are not present in the X-ray pattern. This is a manifestation of the difference in the nature of scattering in the two types of radiation, neutron diffraction being superior to X-ray diffraction in certain respects showing more detailed pattern. From the X-ray pattern, the cell dimension was calculated for several peak positions and the average of them was 8.44$\mathring{A}$. This appears to be slightly bigger than that measured by neutron and is more deviated from the extrapolated value obtained from the curve of Fig.5.2. This is because, the latter was obtained in a more precise method through refinement of the neutron difraction data. Since the X-ray machine in BUET does not produce any diffraction data but produces only a diffraction pattern through chart drive output, it can not be analyzed by computer program. For the same reason it was not possible to measure the oxygen parameter u in the X-ray diffraction method.

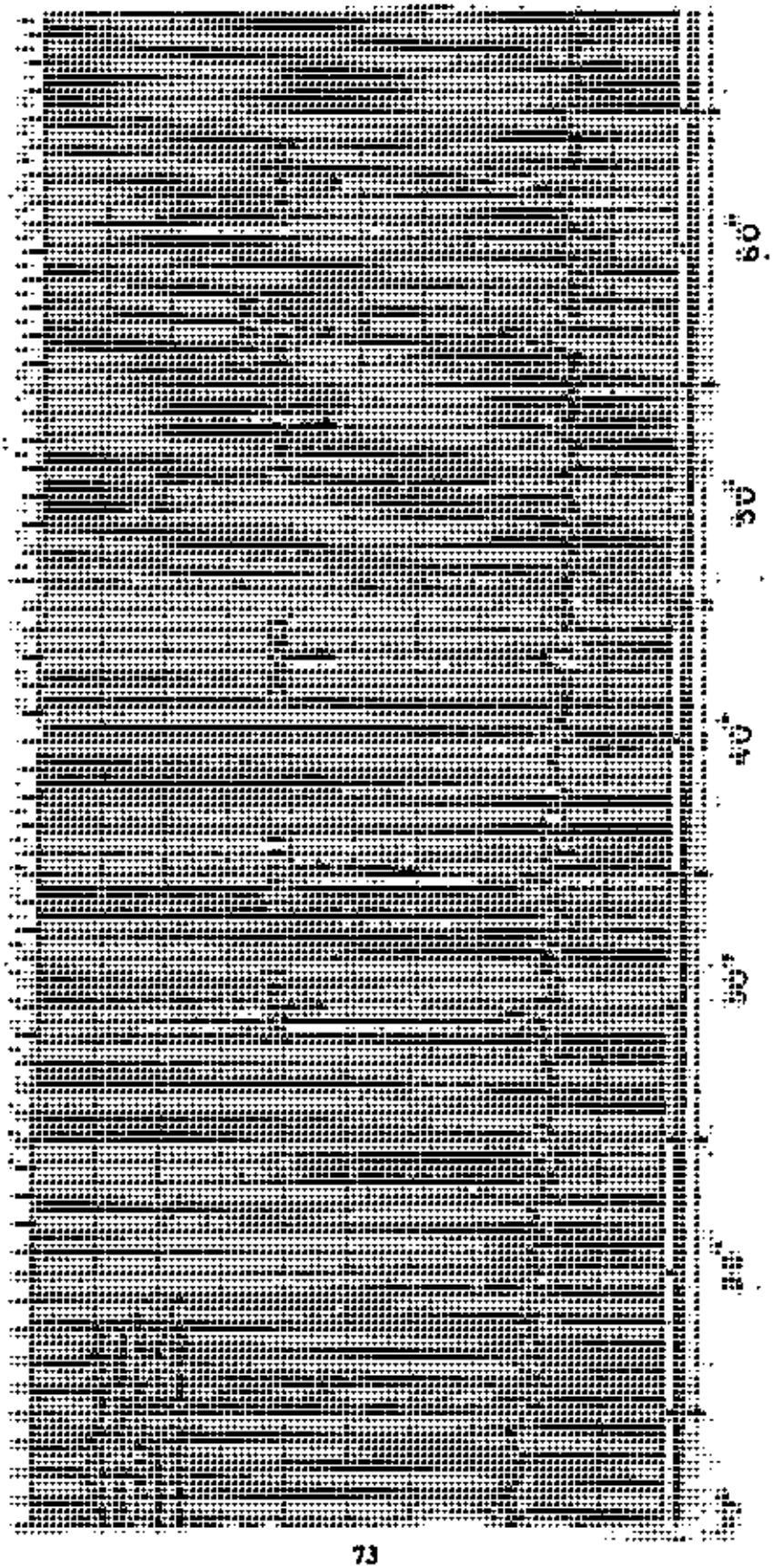


**Fig. 5.3 X-ray Diffraction Pattern of $Zn_{0.5}Ni_{0.5}Fe_2O_4$**

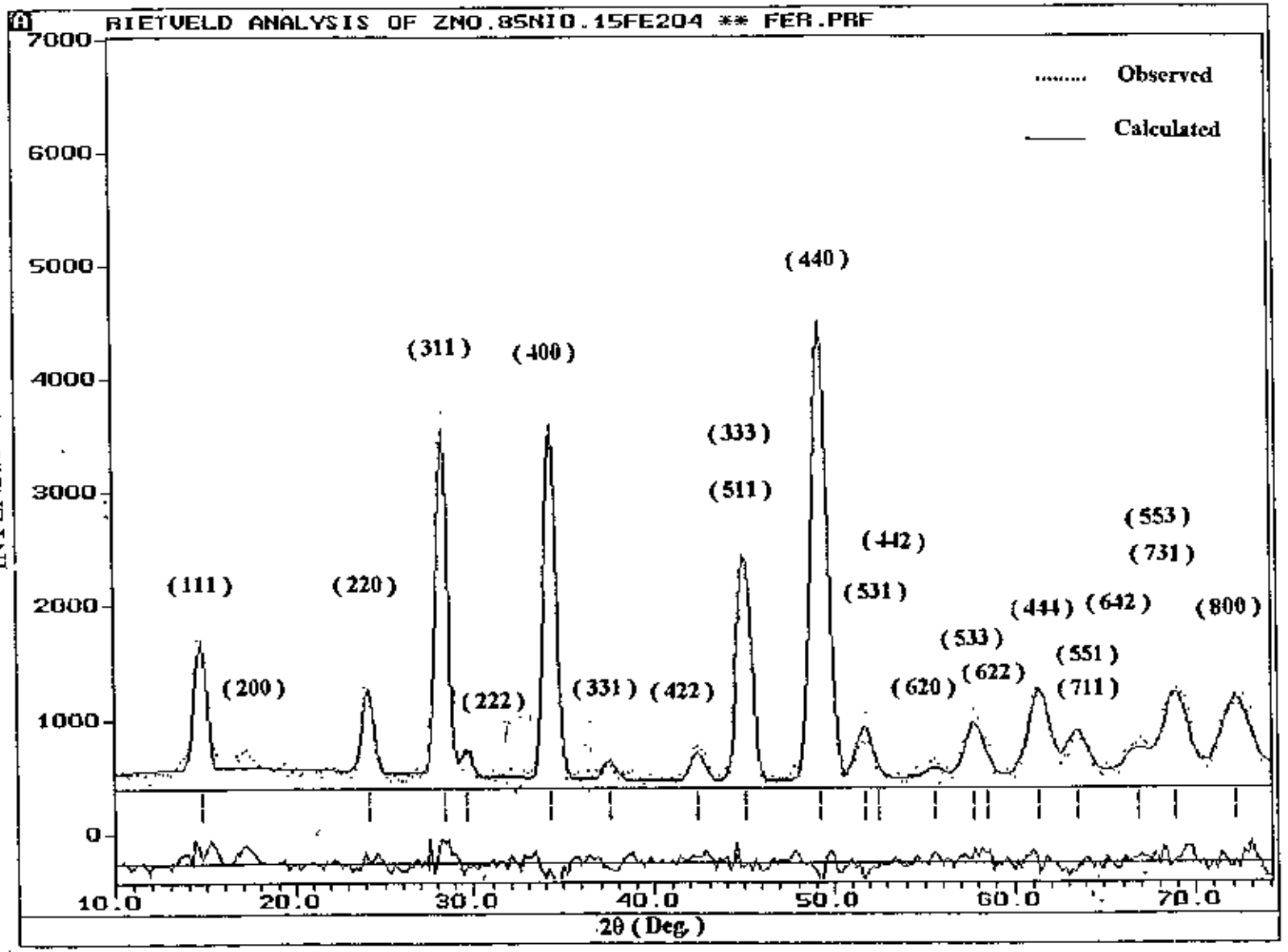


Fig. 5.4 Fitted Neutron Diffraction Pattern of $Zn_{0.85}Ni_{0.15}Fe_2O_4$

## ii) Magnetic Structure:

In the refinement process of the observed diffraction data , the magnetic part was refined in a separate phase. Table 5.5 shows the refined values of the observed and calculated intensity for all the reflections. In the case of ferrites having spinel structure, the magnetic ions with different spin orientations usually occupy non-equivalent crystallographic sites. Hence the magnetic and nuclear Bragg reflections occur at the same angular positions ( $\theta$ ). Such a ferrite system belongs to the space group Fd3m. The data were refined according to this space group and the allowed Bragg reflections in this space group are listed in column 1 in Table 5.5. Fig. 5.4 shows that in the observed diffraction pattern there is existence of ( 200 ) reflection which is extinct in the space group and is absent in Table 5.5. The existence of this superlattice ( 200 ) reflection line is the most striking feature of the Ni-Zn mixed ferrite with higher concentration of zinc, which is a manifestation of the canting of the B site spins. The spin orientation of this ferrite follows the Yafet-Kittel scheme[19] where the B site spin is canted with respect to that of the A site as shown in Fig.5.5. According to this scheme, the normal component of the B site moments gives rise to ( 200 ) super lattice reflection apart from modifying the intensities of the normal reflections. The net moment of B site is still parallel to the moment of A site. The Yafet-Kittel scheme of the ordering of the magnetic moments in such ferrite systems have been treated in details in section 2.5 of chapter 2.

# TABLE 5.5

## Comparison of the refined values of the observed and calculated intensities in the magnetic phase

| ( h k l ) | Multiplicity | Scattering angle ( Deg. ) | Calculated Intensity | Observed Intensity |
|---|---|---|---|---|
| ( 1 1 1 ) | 8 | 14.625 | 19 | 24 |
| ( 2 2 0 ) | 12 | 23.992 | 184 | 190 |
| ( 3 1 1 ) | 24 | 28.212 | 340 | 369 |
| ( 2 2 2 ) | 8 | 29.494 | 137 | 107 |
| ( 4 0 0 ) | 6 | 34.187 | 97 | 90 |
| ( 3 3 1 ) | 24 | 37.363 | 128 | 133 |
| ( 4 2 2 ) | 24 | 42.200 | 49 | 66 |
| ( 5 1 1 ) | 24 | 44.894 | 3 | 3 |
| ( 3 3 3 ) | 8 | 44.894 | 1 | 1 |
| ( 4 4 0 ) | 12 | 49.125 | 45 | 44 |
| ( 5 3 1 ) | 48 | 51.537 | 69 | 55 |
| ( 4 4 2 ) | 24 | 52.323 | 4 | 4 |
| ( 6 2 0 ) | 24 | 55.388 | 14 | 22 |
| ( 5 3 3 ) | 24 | 57.614 | 18 | 21 |
| ( 6 2 2 ) | 24 | 58.344 | 25 | 27 |
| ( 4 4 4 ) | 8 | 61.209 | 11 | 11 |
| ( 7 1 1 ) | 24 | 63.306 | 10 | 7 |
| ( 5 5 1 ) | 24 | 63.306 | 0 | 0 |
| ( 6 4 2 ) | 48 | 66..720 | 11 | 14 |
| ( 7 3 1 ) | 48 | 68.726 | 13 | 15 |
| ( 5 5 3 ) | 24 | 68.726 | 6 | 7 |
| ( 8 0 0 ) | 6 | 72.011 | 3 | 3 |

$R_{magnetic} = 11.2$

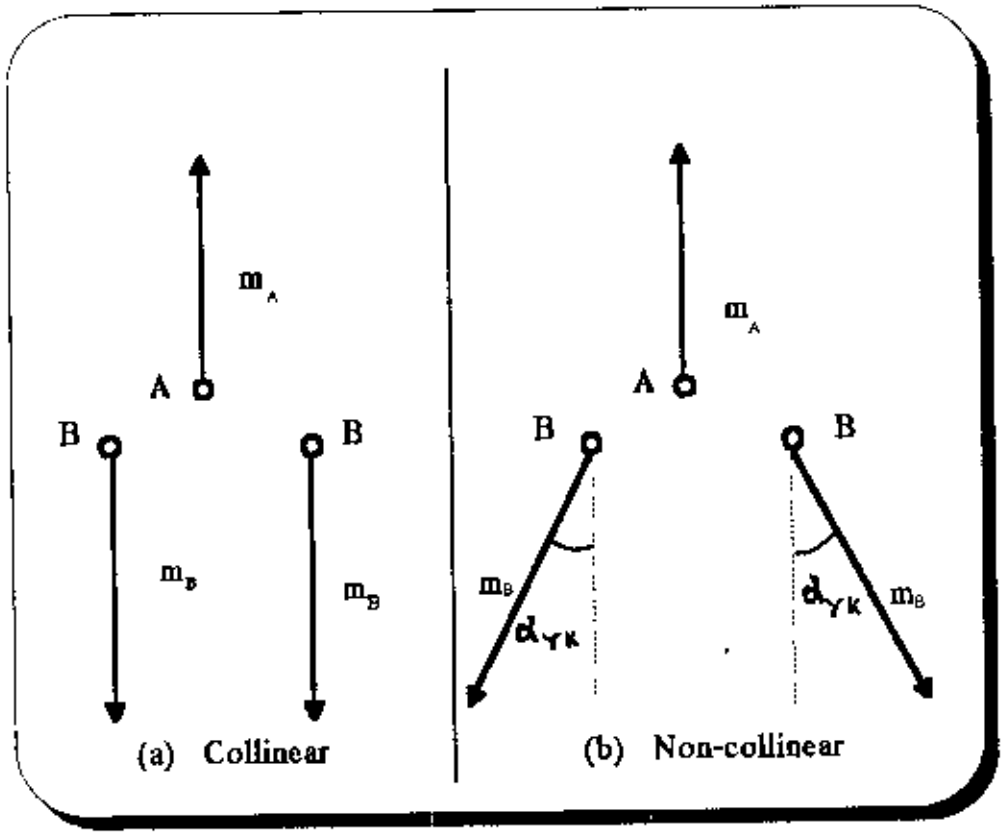


**Fig. 5.5 (a) Collinear and (b) Non-collinear Spin Configuration in Ferrite.**

Usually in a ferrite, AB interaction is much stronger than the AA and BB interactions resulting in a collinear Neel type of coupling between A and B site moments. The nonmagnetic$Zn^{2+}$ ions in a Ni-Zn mixed ferrite enter into the A site and weaken the A site moment but increases the net ferric moment. Because the AB interaction is still stronger and the $Fe^{3+}$ ions in the B site have antiparallell (collinear) moments with that of the remaining $Fe^{3+}$ ions in the A site. If the addition of zinc is continued, then for pure Zn-ferrite, the net moment is expected to be increased up to $10\mu_B$. But it is interesting to note that in practice the net moment is zero.

Guillaud [26] found that the saturation magnetization in Ni-Zn mixed ferrite increases up to about 50 molecular percent of Zn and then starts decreasing. When the A site moment weakens beyond a certain value, the AB interaction will no longer remain stronger. The BB interaction starts dominating and according to Yafet and Kittel the B sublattice splits into two sublattices. The Neel type of collinear spin coupling then disappears and a non-collinear spin ordering results. The direction of the moments of each B sublattice makes an equal angle with the direction of the moment in A sublattice. This angle is called a Y-K angle. As the Zn concentration goes on increasing this Y-K angle also increases and finally at $ZnFe_2O_4$ the angle becomes $90^0$ with an antiferromagnetic configuration of the spins on the B site.

The present sample contains very high concentration of zinc and the spin configuration in this case should definitely follow the Y-K coupling scheme and as discussed above the presence of ( 200 ) supperlattice reflection in the diffraction pattern is a confirmation of this type of spin coupling. The data were refined by the FULLPROF program taking into consideration of

the canted spin in the B site. But the program generated the reflections in the calculated pattern according to the space group Fd3m. The magnetic R-factor $R_{magnetic}$ obtained from the refinement was 11.2 which appears to be somewhat larger. This is because of the fact that the program could not produce the ( 200 ) supper lattice line in the calculated pattern as it is forbidden in the space group and could not fit that reflection. However, the contribution of the normal component of the B site moment to other allowed reflections were duly taken into account by the program. It can be seen from the Table 5.5 that as the magnetic moment of the sample was very small its contribution to the diffracted beam was also very small. Therefore, the poor statistics in the magnetic part of the data was also responsible for high R-factor. The measured moment of atoms at each lattice site and the observed Y-K angle in the B site of the present sample has been shown in table 5.6 along with those of a sample with composition $Zn_{0.75}Ni_{0.25}Fe_2O_4$ studied by N. S. Satya Murthy et al.[9] for comparison. As reported by N S. Satya Muthy and associates out of the four samples with different zinc contents ( x values ) only the above sample possessed Y-K type of moment configuration at room temperature. The sample under present study though has a different zinc content but exhibits the same moment configuration.

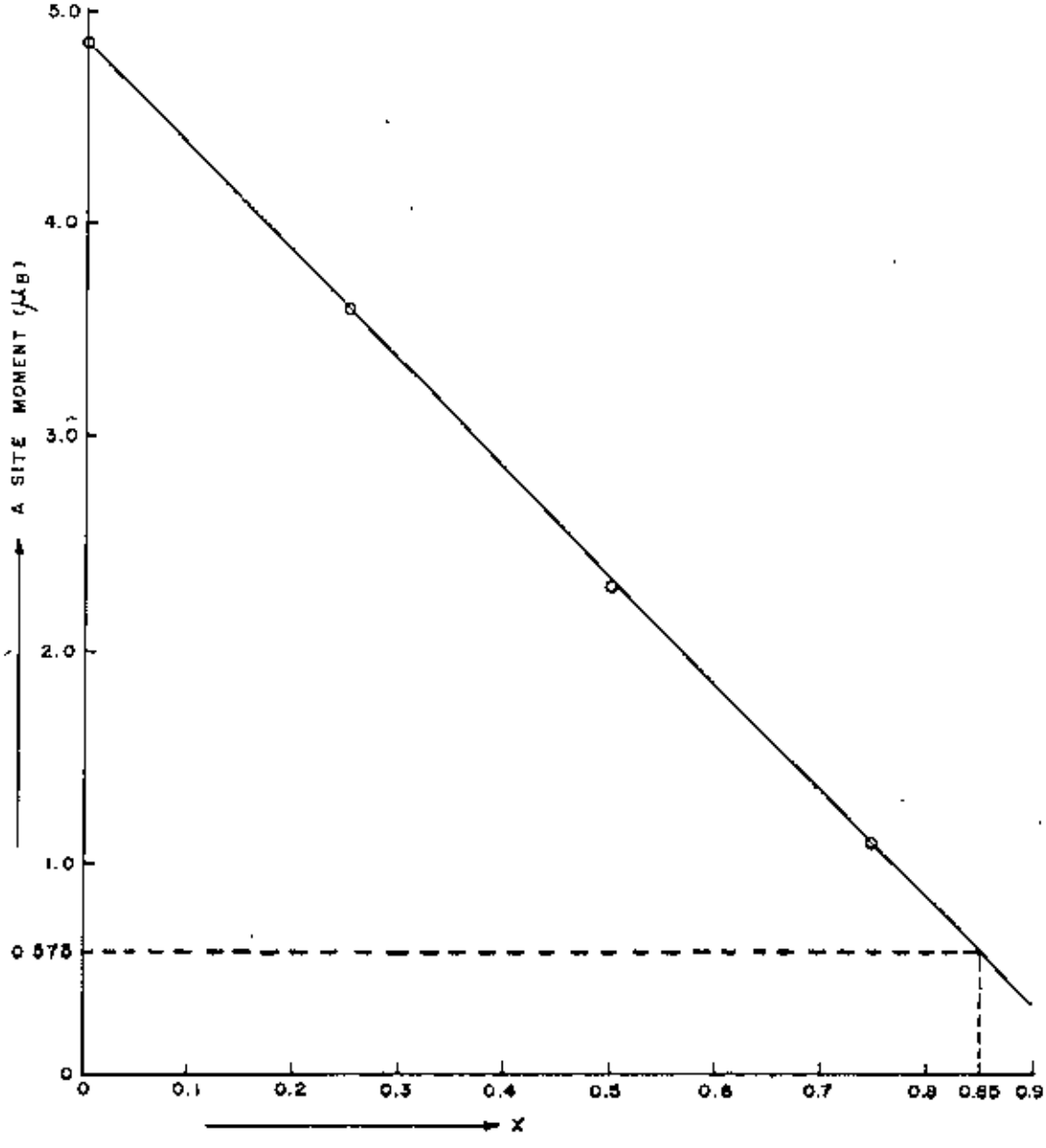


**Fig. 5.6 A Site Moment as a function of x as measured by N. S. Satya Murthy et al.**

# TABLE 5.6

## Comparison of the magnetic moments and Y-K angles of

## $Zn_{0.85}Ni_{0.15}Fe_2O_4$ and $Zn_{0.75}Ni_{0.25}Fe_2O_4$

## ( The moments are in $\mu_B$ )

| SAMPLE | A site moment | Parallel component of B site moment | Normal component of B site moment | Net B site moment | Ferric moment in B site | Net ferric moment per formula unit | Y -K angle |
|---|---|---|---|---|---|---|---|
| $Zn_{0.85}Ni_{0.15}Fe_2O_4$ (Sample under present study) | 0.58 | 0.606 | 1.26 | 1.398 | 1.212 | 0.632 | $64.3^0$ |
| $Zn_{0.75}Ni_{0.25}Fe_2O_4$ [9] | 1.10 | 1.30 | 1.30 | 1.84 | 2.60 | 1.50 | $45^0$ |

The moment in A site gradually dilutes with the increase of concentration of zinc and consequently , the BB interaction also enhances resulting in an increase of Y-K angle. From the Table 5.6, it is seen that in case of the present sample $Zn_{0.85}Ni_{0.15}Fe_2O_4$ the A site moment is $0.58\mu_B$ which is nearly half of that for the sample $Zn_{0.75}Ni_{0.25}Fe_2O_4$. For an increase of zinc content by 10 molecular percent ( x = 0.10 ) in the present sample the Y-K angle has increased by $19.3^0$ ( from $45^0$ to $64.3^0$ ). This indicates a strong dependence of Y-K angle on zinc content. Fig.5.6 shows a plot of A site moment versus x for the four different samples measured by N. S. Satya Murthy et al. From the extrapolation of this curve the A site moment for the present sample ( x = 0.85 ) is found to be $0.575\mu_B$ which is very close to our measured value. The plot for net ferric moment as a function of x for those samples has been presented in Fig. 5.7. Our measured net ferric moment $0.632\mu_B$ agrees very well with the extrapolated value $0.625\mu_B$ for x = 0.85 from this curve.

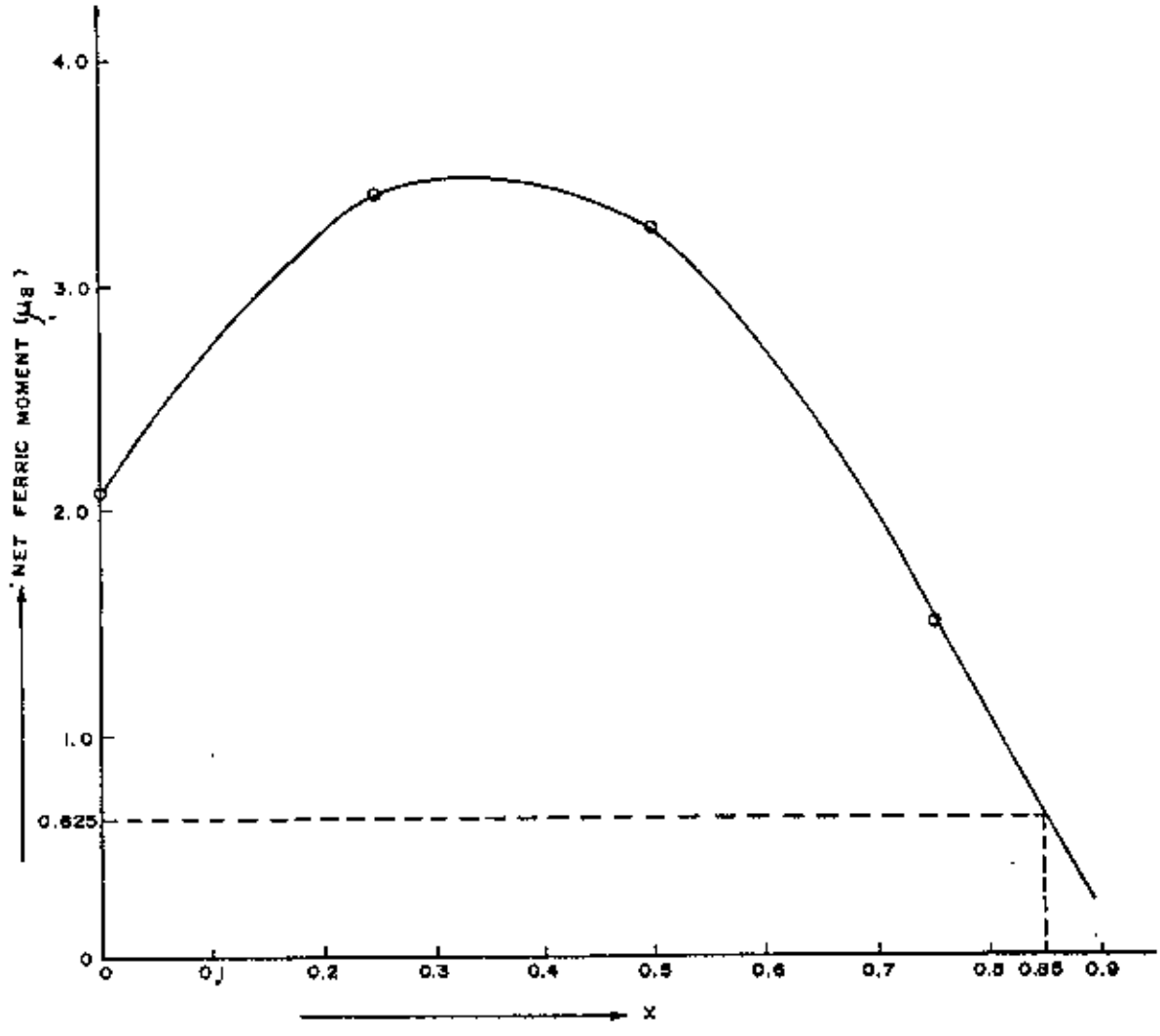


**Fig. 5.7 Net Ferric Moment as a function of x as measured by N. S. Satya Murthy et al.**

# *CHAPTER 6*

## CONCLUSIONS

Neutron diffraction technique is a modern and very useful method for structural studies of crystalline solids, especially, this method is almost unique in the determination of magnetic structure where orientation of atomic moments varies at different crystal lattice sites. The Triple axis neutron spectrometer employed in the present neutron diffraction studies was installed as an annex to the TRIGA MARK II research reactor of Atomic Energy Research Establishment, Savar, Dhaka in 1992. The installation of this machine has opened a neutron diffraction facility in Bangladesh for the first time. It was essential to do necessary alignments of the different axes of the spectrometer as a part of its setting up for performing actual neutron diffraction experiments. It was also essential to verify the reproducibility of diffraction data through neutron diffraction study with a standard sample in order to test the performance of the spectrometer. These were accomplished in the first part of the present study. The monochromator and the detector zero position were aligned properly to select a monochromatic beam of neutron of wavelength 1.24Å. With this set-up of the spectrometer a neutron diffraction run from $25^0$ to $82^0$ with standard powdered aluminium sample was taken. The obtained data was analyzed by a Rietveld refinement program. As shown in chapter 5 the performance of the spectrometer after the final setting is quite satisfactory. This is reflected in the good correspondence between observed and calculated intensities and between the measured cell dimension and its value quoted in the literature. This provided the calibration and checking of the spectrometer.

In the second part of the present study both the crystal and magnetic structure at room temperature of a Ni-Zn ferrite were determined from the neutron diffraction measurement. The present experiment of determining the magnetic structure of a ferrite sample by neutron diffraction was the first of its kind in Bangladesh. A neutron diffraction experiment from $10^0$ to

$74.4^0$ of a ferrite sample of composition $Zn_{0.85}Ni_{0.15}Fe_2O_4$ was done at room temperature. The obtained data were analyzed by a computer program FULLPROF in the Rietveld method. The nuclear and magnetic contributions in the diffracted intensity were analyzed separately in two different phases. The cell dimension and the oxygen parameter u were found out in the first phase of the refinement. The magnitude and orientation of atomic moments of the atoms in different crystal lattice sites were determined in the second phase of the refinement which provided the magnetic structure of the sample under study. It had been found that the sample possessed a Y-K type of spin configuration at room temperature. A comparison of the determined crystal structure parameters and magnetic moments in A and B sites along with the Y-K angle formed by the moment in the B site with the similar work on samples of slightly different composition done by other authors had been shown in chapter 5. Our measured values were found to be reasonably in good agreement with those.

As, this was the first neutron diffraction experiment in the country many constraints were there. Neutron diffraction experiment is usually very time consuming and the time factor is closely related to the reactor flux and the time of operation of the reactor. Although, the neutron flux at the reactor core is of the order of $10^{13}$ $n.cm^{-2}$ $sec^{-1}$ but at the sample position in the spectrometer, the flux is of the order of $10^5 n.cm^{-2}sec^{-1}$. Due to this low neutron flux we had to set a longer counting time for the detector at each scanning step to make the counting statistics reasonably good. This made the experimental time long. Again due to some technical difficulties the reactor could not be in operation every day and also could not run for a long time on the days of the operation. So, the completion of a single diffraction run took more than a month. Again for powdered aluminium sample we had to take empty container scan in order to subtract its

contribution in the observed data and for Ni-Zn ferrite we took two sets of diffraction data for clarity. In the present technique, the data analysis process is rather lengthy , because one can not get a very good agreement between observed and calculated pattern unless one starts with parameters which are very close to the actual values. Thus we had to follow itinerant process of successive convergence to the actual value. Because of this lengthy nature of the present technique it has not been possible to study the various compositions of Ni-Zn ferrite as one would like.

There was no facility for on-line low temperature neutron diffraction measurements in the Triple axis neutron spectrometer used in the present study. Hence, neutron diffraction pattern at low temperature could not be looked for. Satya Murthy et al.[9] showed that any Ni-Zn mixed ferrite containing more than 75 molecular percent of zinc does not have any Neel temperature and possesses Y-K type spin configuration at all temperatures. Due to lack of low temperature facilities the possibility of having Neel type of ordering and a corresponding Neel temperature could not be verified for the sample under present study. Furthermore, there was no facility in the spectrometer to do neutron diffraction measurements under magnetic fields which would give us the opportunity to observe the effects of magnetic field on the ordering of the magnetic moments in this sample.

# REFERENCES


1. G. E. Becon, Neutron Diffraction 3rd Edition, Clarendon Press: Oxford ( 1977 ).
2. W. Marshall and S. W. Lovesy, Theory of Thermal Neutron Scattering, Clarendon Press: Oxford, ( 1971 ).
3. B. T. M. Willis, Thermal Neutron Diffraction, Oxford University Press, ( 1968 ), Chemical Applications of Thermal Neutron Scattering, Oxford University Press ( 1971 ).
4. C. G. Shull, W. A. Strauser, and E. O. Wollan. Phys. Rev. 83, 333 (1951).
5. C. G. Shull and M. K. Wilkinson, Rev. Mod. Phys. 25, 100 ( 1953).
6. J. L. Snoek, Philips Technical Review, 8, 353 (1946 ).
7. J. M. Hastings and L. M. Corliss, Phys. Rev. 104, 328 (1956).
8. J. M. Hastings and L. M. Corliss, Rev. Mod. Phys. 25, 114 (1953 ).
9. N. S. Satya Murthy, M. G. Natera, S. I. Youssef, R. J. Begum and C. M. Srivastava, Phys. Rev. 181, 969 (1969).
10. Y. Yafet and C. Kittel, Phys. Rev. 87, 290 (1952 ).
11. L. Neel, Ann. Phys. 3, 137 (1948).
12. J. C. Slater. Phys. Rev. 35, 509, (1930 ).
13. J. C. Slater. Phys. Rev. 36, 57, ( 1930 ).
14. A. Sommerfeld and H. Bethe, Handbach der Physik. 24, ( part II ). 595, ( 1933 ).
15. H. A. Kramer, Physica, 1, 182 (1934 ).

16. P. W. Anderson, Phys. Rev. 115, 2 (1959 ).

17. J. H. Van Vleck, J. phys. Radium, 12, 262 (1951).

18. P. K. Lotgering, Philips Res. Repts. 11, 190 (1956).

19. E. Prince, Acta Cryst. 10, 554 (1957).

20. H. M. Rietveld, Acta Cryst. 20, 508 (1966 ).

21. H. M. Rietveld, Acta Cryst. 22, 151 (1967 ).

22. G. Caglioti, A. Paoletti and F. P. Ricci, Nucl. Instrum. 3, 223, ( 1958 ).

23. A. W. Hewat, Harwell Report (unpublished) RRL 73/239 (1973 ).

24. R. W. G. Wyckoff, Crystal Structures, Vol. 1, 2nd Edition ( 1960 )

25. V. C. Wilson and J. S. Kasper, Phys. Rev. 95, 1408 ( 1954 ).

26. C. Guillaud, J. Phys. Radium 12, 239 (1951).